Delay-Trajectory-Accuracy Trilemma Optimization for Non-IID Mitigation in UAV-Cooperative Federated Learning IoT

Qihao Li, *Member, IEEE*, Tongzhou Yang, Qiang Ye, *Senior Member, IEEE*, Nan Cheng, *Senior Member, IEEE*, Fengye Hu, *Senior Member, IEEE*

***Abstract*—In this paper, we propose a novel cooperative-enabled communication and learning optimization (CCLO) scheme to resolve the delay-trajectory-accuracy trilemma for non-independent and identically distributed (non-IID) data mitigation in UAV-assisted federated learning (FL) for IoT networks. Specifically, we design a tri-modular framework that synergizes dynamic blocklength allocation, energy-aware trajectory planning, and reliability-driven weight adaptation. We derive a convex reformulation of the error probability minimization problem by exploiting temporal coupling between UAV mobility and blocklength allocation, enabling real-time adaptation to channel dynamics via the golden section algorithm. Then, we develop a successive convex approximation (SCA)-based trajectory optimizer with novel convex relaxations to address non-convex collision avoidance and energy constraints. By introducing auxiliary distance variables, we decouple spatial and spectral resource dependencies, achieving Pareto-optimal paths that balance flight energy and latency. We investigate decentralized weight coordination through a block-coordinate Gauss-Seidel algorithm, dynamically aligning aggregation weights with channel success probabilities and local model divergence metrics to counteract stochastic packet losses. The closed-loop interaction among trajectory planning, blocklength allocation, and weight adaptation together ensures FL convergence while mitigating non-IID data skew and resource constraints. Simulation results demonstrate that the CCLO scheme significantly reduces communication delay and improves model accuracy by 18.9% compared to benchmarks. It also maintains robust convergence under time-varying wireless channels and diverse device distributions, validating its efficacy in harmonizing the trilemma for UAV-cooperative FL-IoT systems.**

I. Introduction

THE widespread deployment of Internet of things (IoT) devices has led to the increased adoption of federated learning (FL), which allows collaborative model training to be performed while data privacy is preserved [1]–[3]. However, data heterogeneity across IoT devices is observed to degrade model convergence and accuracy. This non-independent and identically distributed (non-IID) characteristic of data is often associated with model overfitting and inconsistencies in the FL global model performance [4], [5]. Recent studies suggest using unmanned aerial vehicles (UAVs) as mobile relays to address these issues in FL deployment, with their spatial mobility aiding in data diversity and improving communication and learning efficiency by adapting to real-time conditions [1], [6]. While UAV-assisted FL offers promise, cooperating UAVs with ground devices introduces complex tradeoffs among communication delay, trajectory energy costs, and model accuracy. The interdependence of these variables—where minimizing delay increases energy consumption, while trajectory adjustments impact channel states and aggregation weights—leads to a high-dimensional, non-stationary optimization landscape requiring joint convex reformulation and distributed coordination. Existing works often address subsets of this issue: for instance, [7] optimizes UAV paths to minimize latency but overlooks energy constraints, while [8] balances energy and accuracy but assumes static channels.

However, resolving this trilemma necessitates addressing three interconnected challenges rooted in the interdependence of mobility, channel dynamics, and distributed coordination. The first challenge lies in time-varying channel-state coupling, where optimal blocklength allocation must adapt to dynamic channel conditions induced by UAV mobility and fading effects. Traditional methods for latency reduction in UAV-assisted networks predominantly rely on static resource allocation strategies, such as fixed power distribution or bandwidth partitioning, which often fail to adapt to dynamic channel conditions. In addition, conventional blocklength allocation methods, which were designed for quasi-static channels, are not efficient for the rapid signal-to-interference-plus-noise ratio (SINR) variations that are caused by UAV movement. These variations can be observed when Doppler effects interfere with channel estimation or when line-of-sight (LoS) connections are repeatedly interrupted, resulting in inconsistent packet transmission [9]. To overcome these limitations, real-time blocklength adaptation mechanisms are essential to ensure communication reliability for FL updates, bridging the gap between theoretical channel capacity and practical UAV-assisted FL deployment.

The second challenge arises from the energy-delay-accuracy trilemma under non-convex mobility constraints. The optimization of UAV trajectories requires balancing multiple objectives: flight energy consumption must be minimized, communication latency must be reduced, and data diversity must be maximized to address non-IID data distributions [10]. Dynamic path adjustments are implemented to balance spatial data coverage and energy efficiency. More aggressive flight paths provide better data representation but consume more battery power, while more conservative routes are observed to increase transmission delays and potentially introduce model bias [11], [12]. Moreover, to address non-IID data distribution, UAVs must be deployed across diverse device clusters for balanced local dataset representation. However, these extended

coverage paths are associated with increased energy consumption and communication delays. Prior works like [13] employ deep reinforcement learning (DRL) for energy-aware path planning but ignore latency-accuracy interdependencies. Thus, it is necessary to produce a holistic approach to jointly optimize trajectories with energy budgets, channel dynamics, and FL convergence thresholds.

The third challenge involves the stochastic correlation between aggregation weights and communication reliability in distributed UAV-assisted networks. FL performance depends on both data quality (local model accuracy) and update delivery reliability. For instance, UAV mobility combined with dynamic interference patterns can result in unpredictable reduced data reliability, hence causing significant discrepancies between local updates and the aggregated global model. Biased weighting schemes—such as those ignoring packet loss rates [14] —amplify model divergence, while decentralized coordination without synchronization risks update staleness [15]. The FedProx method [16] incorporates a proximal term to limit divergence in heterogeneous environments. Control variates are utilized by the SCAFFOLD method [17] to reduce client drift. Additionally, local updates are normalized by the FedNova method [18] to address gradient staleness and objective inconsistency issues. Although these approaches significantly improve convergence rates with non-IID data and irregular participation patterns, they operate under the assumption of flawless data transmission and consequently remain susceptible to packet loss in wireless networks. Novel mechanisms are required to dynamically adjust weights based on real-time channel states and model utility, ensuring robust aggregation in presence of intermittent connectivity.

In this paper, we focus on resolving the intertwined challenges of communication delay, UAV trajectory, and FL model accuracy in UAV-assisted FL for IoT networks. We propose a cooperative-enabled communication and learning optimization (CCLO) scheme, which is a tri-modular framework that synergizes dynamic blocklength allocation, energy-aware trajectory planning, and reliability-driven weight adaptation. The three modules exchange parameters accordingly: the dynamic blocklength optimization module feeds channel-adaptive blocklengths to the UAV trajectory optimization module, which uses these to compute energy-minimal paths. The resulting reliability metrics and communication error rate are then relayed to the local update weight adjustment module, which dynamically tunes aggregation weights based on both link reliability and local model divergence metrics. This closed-loop interaction ensures FL convergence while balancing non-IID mitigation. The primary contributions are threefold.

- First, we investigate the temporal coupling between UAV mobility and blocklength allocation, deriving a convex reformulation of the error probability minimization problem. By exploiting the concavity of the composite function and leveraging the golden section algorithm, we achieve real-time blocklength adaptation that reduces the retransmission overhead.
- Second, we develop a successive convex approximation (SCA)-based trajectory optimizer with novel convex relaxations for non-convex collision/energy constraints. By introducing auxiliary distance variables, we decouple spatial and spectral resource dependencies, enabling Pareto-optimal trajectories that reduce energy consumption while maintaining pre-determined thresholds.
- Third, we investigate decentralized weight coordination, where dual variables are computed via bisection to enforce reliability-aware aggregation. This mechanism reduces model divergence under stochastic packet losses by aligning weights with both channel success probabilities and data quality metrics.

II. Literature Review

Various schemes have been investigated to address the challenges of cooperation-based communication and learning optimization in UAV-assisted networks. While existing works provide valuable insights into individual aspects of these problems, critical gaps remain in addressing the inherent interdependencies among channel-state variations, energy constraints, and model aggregation complexity.

Recent advancements in adaptive blocklength optimization have demonstrated promising approaches to mitigate latency in UAV-assisted networks. Cheng et al. proposed an adaptive blocklength optimization framework using proximal ADMM and deep Q-learning to balance transmission and queuing delays, minimizing latency in wireless communication [19]. An achievable rate formula for finite blocklength transmission was introduced for maximizing weighted sum rate, energy efficiency, and user fairness in uRLLC systems [20]. Liu et al. formulated a joint optimization problem for UAV-assisted transmission, optimizing UAV power and trajectory to maximize secrecy rate while addressing covert communication constraints using alternating optimization and SCA [25]. Although adaptive transmission strategies offer significant improvements in terms of blocklength optimization, they generally rely on idealized assumptions, such as perfect CSI estimation and predictable UAV mobility. In highly dynamic environments, such as those involving rapidly changing interference conditions, these solutions often struggle to maintain reliability.

Trajectory optimization to minimize communication latency often leads to conflicts with energy consumption and FL convergence requirements, especially when the UAV must make aggressive trajectory adjustments to improve data distribution. Studies [21] have proposed genetic algorithm (GA) and successive convex approximation (SCA) methods for UAV trajectory planning, addressing data collection, obstacle avoidance, and energy constraints. However, the non-convex nature of UAV mobility complicates optimization, as minimizing latency often conflicts with energy and FL convergence deadlines. Qin et al. [22] tackled energy-efficient trajectory optimization using Lyapunov optimization, but aggressive adjustments can deplete UAV battery resources and exacerbate non-convexity, leading to inefficient resource utilization.

Beyond physical layer and mobility challenges, the inherent data heterogeneity in UAV-assisted FL systems introduces fundamental barriers to reliable model convergence. Algorithm-centric non-IID mitigation approaches such as FedProx, SCAFFOLD, and FedNova [16]–[18] reshape the

TABLE I. Comparative positioning of representative prior works versus the proposed CCLO framework.

Category / Representative Work	Traj.	Rate Adapt.	Res. Alloc.	R-C	Non-IID	M-Domain	BL Explicit	RW
Adaptive blocklength & latency (e.g., [19], [20])	–	✓	O	NR	–	–	✓	–
UAV path / energy optimization (e.g., [21], [22])	✓	–	O	NR	–	–	–	–
Non-IID FL algorithms (e.g., [16]–[18])	–	–	–	NR	✓	–	–	–
Reliability / packet-loss aware FL (e.g., [23], [24])	–	O	–	O	–	–	O	O
CCLO (this work)	✓	✓	O	✓(closed loop)	✓(RW)	✓	✓	✓

Note: ✓= explicitly addressed; – = not addressed; O = indirectly / partially addressed; FB = finite-blocklength considered; NR = addressed without explicit reliability–convergence coupling; RW = reliability-aware weighting; M-Domain = Joint Multi-Domain (Traj+BL+Weight); R-C = Reliability-Convergence Coupling.

optimization dynamics via proximal regularization, control variates, or normalized updates. Specifically, Li et al, extended FedAvg by adding a proximal term to stabilize training and improve convergence in heterogeneous federated networks [16]. Karimireddy et al. introduced control variates to mitigate client drift, enhancing convergence speed under non-IID data distributions [17]. Wang et al. proposed normalized update aggregation to fairly combine client updates despite varying local computation and data heterogeneity [18]. However, the challenge remains in balancing both data quality and communication reliability, as biased weight adjustments can destabilize FL convergence, leading to inconsistent model updates across UAVs and devices. Distributed systems that operate without centralized synchronization often suffer from delays, hindering real-time model improvements and convergence.

Research on reliability-aware and packet-loss mitigation in FL [23], [24] systematically analyzes how stochastic transmission failures and device unavailability affect convergence performance. Xiang et al. [23] modeled packet loss probabilities in FL over unreliable mobile edge networks, linking them to convergence performance. Balasubramanian et al. [24] addressed reliability-aware federated learning by incorporating probabilistic participation and fault-tolerant scheduling mechanisms in time-sensitive networks, analyzing the effect of stochastic node failures on convergence. These studies introduce probabilistic participation models and establish connections between reliability metrics and scheduling protocols. However, these approaches focus on scheduling mechanisms rather than developing comprehensive bounds based on finite-blocklength, which could enable continuous joint optimization of both communication parameters and aggregation strategies.

While significant progress has been made in blocklength optimization, UAV trajectory planning, and distributed model aggregation, these approaches remain limited when implemented in the dynamic environments of UAV-enabled communication systems. Questions remain open regarding time-varying channel-state relationships, the balance between energy, delay, and accuracy requirements, and the statistical patterns in distributed federated learning environments. Through these investigations, explicit trade-offs between latency, energy consumption, link reliability, and statistical drift can be established, enabling the networking layer to directly influence learning dynamics in these systems. In this paper, our target is to optimize communication efficiency, ensure reliable model convergence, and balance resource allocation while considering the dynamic and unpredictable nature of the system. Please refer to Table I for comparison details among the existing works and the proposed CCLO scheme.

III. SYSTEM MODEL

A. Network Model

As shown in Fig. 1, the network is composed of three key components: a base station (BS), M IoT devices and N UAVs. Denote by $\mathbf{D}$ the IoT devices subset and $\mathbf{U}$ the UAVs subset, collectively forming the disjoint set $\mathbf{S_{all}} \triangleq \mathbf{D} \cup \mathbf{U}$, where the number of elements in $\mathbf{S_{all}}$ is $c(\mathbf{S_{all}}) = M + N$. The BS is equipped with a central server (CS) $\mathbf{c}$, which is responsible for aggregating model updates and refining global model parameters during the federated learning process. Additionally, the BS incorporates a laser-based energy harvesting system $\mathbf{l}$, which wirelessly powers the UAVs. Note that downlink transmissions from the BS are assumed to be error-free due to its high transmission power. IoT devices are equipped with sensors and data acquisition systems to gather diverse types of data from their environments. FL local model training is performed by the devices using the collected data. The UAVs collect and process data from their flight trajectory, updating their own model parameters. These UAV-updated parameters are shared with the paired IoT devices. UAVs act as cooperative nodes between IoT devices and the BS, bridging the communication gap in scenarios where direct device-to-server (D2S) communication is unreliable. They facilitate device-to-UAV (D2U) and UAV-to-server (U2S) transmissions, overcoming connection challenges.

In the FL process, IoT devices, the BS, and UAVs collaborate to exchange and refine model parameters, constructing a globally optimized model. When link quality deteriorates due to factors like distance or interference, the UAV is deployed as a cooperative node to ensure reliable communication. Denote by $\{(i,j) \in \mathcal{P} | 1 \le i \le M, 1 \le j \le N\}$, the cooperative pair between IoT device i and UAV j. In such cases, IoT devices transmit only local information and model updates to the UAV, which then adjusts its trajectory to optimize the FL process and transmission performance. The UAV also shares updated model parameters, derived from its trajectory data, with the paired IoT devices to enhance overall efficiency.

B. Communication Model

In a three-dimensional (3D) Cartesian coordinate system, IoT device i is positioned at $\mathbf{p}_{\text{iot}}^{i} = (x_{\text{iot}}^{i}, y_{\text{iot}}^{i}, 0)$, representing its location on the horizontal plane with zero elevation. The laser transmitter is situated at $\mathbf{p}^{\mathbf{l}} = (x^{\mathbf{l}}, y^{\mathbf{l}}, 0)$, while the CS, which performs model aggregation and parameter updates,

This article has been accepted for publication in IEEE Transactions on Mobile Computing. This is the author's version which has not been fully edited and content may change prior to final publication. Citation information: DOI 10.1109/TMC.2026.3656974

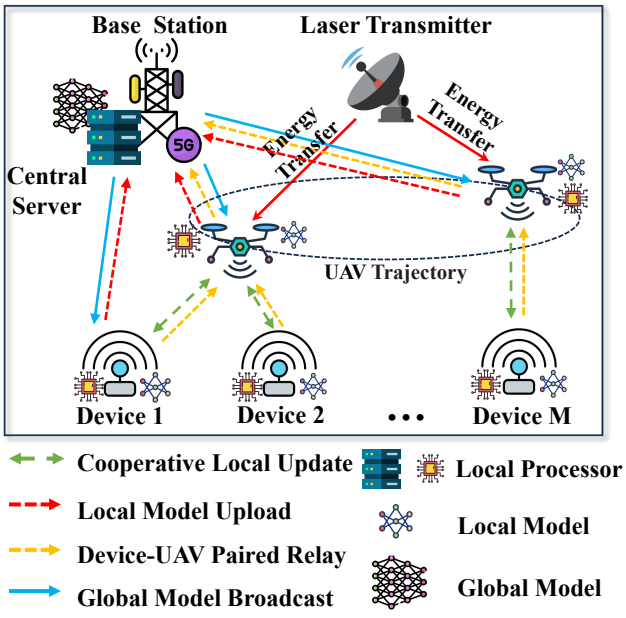

Fig. 1. Network Model.

is located at $\mathbf{p}^{\mathbf{c}} = (x^{\mathbf{c}}, y^{\mathbf{c}}, 0)$. These positions establish the spatial layout of the network, enabling precise modeling of communication links, power transfer mechanisms, and collaborative interactions within the system. At the time instant $t \in \{1, \ldots, T\}$, the UAV j operates at a fixed altitude $H > 0$ and executes horizontal movement within the network. Denote the UAV trajectory position projected on the horizontal plane as $\mathbf{q}^j_{\text{uav}}[t] = [x^j_{\text{uav}}[t], y^j_{\text{uav}}[t], H]^T \in \mathbb{R}^{3\times 1}$, where $x^j_{\text{uav}}[t]$ and $y^j_{\text{uav}}[t]$ represent its horizontal coordinates at time t, and H remains constant to ensure stable flight dynamics and predictable communication patterns. The UAV's trajectory is characterized by its initial position $(x^j_{\text{uav}}[0], y^j_{\text{uav}}[0], H)$ and final position $(x^j_{\text{uav}}[T], y^j_{\text{uav}}[T], H)$. These positions are crucial for optimizing the UAV's flight path to maximize communication reliability, reduce latency, and enhance the efficiency of the overall federated learning process. The distance between the UAV j and the laser transmitter at time t is $\mathbf{d}^{j,\mathbf{l}}_{\text{uav}}[t] = (\|\mathbf{q}^j_{\text{uav}}[t] - \mathbf{p}^{\mathbf{l}}\|^2 + H^2)^{1/2}$. Similarly, the distance between the UAV j and the CS at time t is $\mathbf{d}^{j,c}_{\text{uav}}[t] = (\|\mathbf{q}^j_{\text{uav}}[t] - \mathbf{p}^{c}\|^2 + H^2)^{1/2}$. The velocity of UAV j at time t is defined as: $\|\mathbf{v}^j_{\text{uav}}[t]\| = (\|\mathbf{q}^j_{\text{uav}}[t+1] - \mathbf{q}^j_{\text{uav}}[t]\|)/\Delta^{\text{uav}}_t$, where Δ^{uav}_t represents the time duration during which the UAV changes its position. The UAV's velocity is constrained by its maximum allowable velocity, $V_{\max}$, such that: $\|\mathbf{v}^j_{\text{uav}}[t]\| \leq V_{\max}$. The model parameters generated by loT devices and UAVs are encapsulated in data packets of size L_{pkt} bits, with their transmission required to be completed within the maximum allowable duration, denoted as $T_{\max}$ seconds. The total blocklength is $M_{\text{tot}} = B \times T_{\max}$, where B is the wireless bandwidth. The expression ensures that the transmission adheres to the timing constraints of the network. The packet error rate (PER), ϵ, is a critical metric that quantifies the likelihood of unsuccessful data delivery due to channel impairments, which can be calculated as $\epsilon(\gamma, l) = Q(\ln 2\sqrt{\frac{l}{\Gamma(\gamma)}}(\log_2(1+\gamma-\frac{L_{\text{pkt}}}{l})))$, where l denotes the blocklength, γ is the signal-to-noise ratio (SNR) at the receiver, and $Q(\cdot)$ is the Gaussian Q-function. The Q-function, $Q(a) = \frac{1}{\sqrt{2\pi}}\int_a^\infty e^{-t^2/2}\text{d}t$, measures the tail probability of a standard normal distribution [26], [27]. Additionally, $\Gamma(\gamma) = 1 - (1+\gamma)^{-2}$ is used to model the wireless communication channel variability, accounting for the relationship between SNR and the blocklength.

The communication between an IoT device i and an UAV j at time t is modeled as a Bernoulli random variable $\varphi^{\text{D2U}}_{i,j}(t)$, where $\varphi^{\text{D2U}}_{i,j}(t) = 1$ indicates a successful transmission, and $\varphi^{\text{D2U}}_{i,j}(t) = 0$ represents a failed transmission. The probability of a successful transmission at time t is denoted by $\text{P}^{\text{suc}}_{i,j}\left(\gamma_{i,j}[t], l^{\text{D2U}}_{i,j}[t]\right) = 1 - \epsilon\left(\gamma_{i,j}[t], l^{\text{D2U}}_{i,j}[t]\right)$, where $l^{\text{D2U}}_{i,j}[t]$ specifies the blocklength allocated to the D2U link at time t and $\gamma_{i,j}[t]$ is the SNR for the communication link between IoT device i and UAV j. Here, $\gamma_{i,j}[t] = p^{\text{D2U}}_{i,j}[t]h_{i,j}[t]$, where $p^{\text{D2U}}_{i,j}[t]$ represents the transmission power allocated to the D2U link, and $h_{i,j}[t]$ is the channel gain depending on the distance between IoT device i and UAV j, as well as the altitude of the UAV. If the UAV lies outside the IoT device's communication range, we have $\text{P}^{\text{suc}}_{i,j}(\cdot) = 0$. Specifically, in scenarios involving UAVs, the wireless channel is influenced by both LoS and non-line-of-sight (NLoS) conditions, as well as dynamic environmental factors, which can be defined as

$$h_{i,j}[t] = \frac{\beta_0}{|\mathbf{q}^j_{\text{uav}}[t] - \mathbf{p}^i_{\text{iot}}|^2 + H^2} \cdot e^{-\kappa|\mathbf{q}^j_{\text{uav}}[t] - \mathbf{p}^i_{\text{iot}}|}, \quad (1)$$

where the exponential term $e^{-\kappa|\mathbf{q}^j_{\text{uav}}[t] - \mathbf{p}^i_{\text{iot}}|}$ captures additional attenuation over longer distances due to NLoS effects and environmental factors, β_0 is the channel power gain at a reference distance $d_0 = 1$ meter, $|\mathbf{q}^j_{\text{uav}}[t] - \mathbf{p}^i_{\text{iot}}|$ is the horizontal distance between the loT device i and the UAV j at time t, κ is the environmental attenuation factor which accounts for signal degradation due to NLoS conditions, obstacles, or atmospheric absorption. Note that, by tuning κ, the model can adapt to varying wireless environmental conditions. Assume that the success probability for the U2D transmission is equivalent to that of the corresponding D2U link, such that $\text{P}^{\text{suc}}_{i,j}(\cdot) = \text{P}^{\text{suc}}_{j,i}(\cdot)$. Denote by $\varphi_{j,\mathbf{c}}(t)$ a Bernoulli random variable, where $\varphi^{\text{U2C}}_{j,\mathbf{c}}(t) = 1$ indicates a successful transmission with $\varphi^{\text{U2C}}_{j,\mathbf{c}}(t) = 0$ for failure communication between UAV j and CS at time t. The success probability is given by $\text{P}^{\text{suc}}_{j,\mathbf{c}}(\gamma_{j,c}[t], l^{\text{U2C}}_{j,\mathbf{c}}[t])$, where $\gamma_{j,\mathbf{c}}[t] = p^{\text{U2C}}_{j,\mathbf{c}}[t]h_{j,\mathbf{c}}[t]$, $p^{\text{U2C}}_{j,\mathbf{c}}[t]$ is the transmission power for U2C communication. For notational simplicity, we use $\text{P}^{\text{suc}}_{i,j}$ to represent the success probability $\text{P}^{\text{suc}}_{i,j}\left(\gamma_{i,j}[t], l^{\text{D2U}}_{i,j}[t]\right)$, while $\text{P}^{\text{suc}}_{j,\mathbf{c}}$ denotes the success probability $\text{P}^{\text{suc}}_{j,\mathbf{c}}\left(\gamma_{j,\mathbf{c}}[t], l^{\text{U2C}}_{j,\mathbf{c}}[t]\right)$ for a direct U2C transmission.

The energy consumed by UAV j for communication at time t comprises the energy for U2D communication and U2C communication, which can be expressed as

$$\text{Er}^s_j[t] = \sum_{(j,i)\in\mathcal{P}} \frac{1}{\eta_{j,i}} p^{\text{U2D}}_{j,i}[t]\zeta_{j,i}[t]\Delta^{\text{U2D}}_t + \frac{1}{\eta_{j,\mathbf{c}}} p^{\text{U2C}}_{j,\mathbf{c}}[t]\zeta_{j,\mathbf{c}}[t]\Delta^{\text{U2C}}_t, \quad \forall t \in \{1, \ldots, T\}, \quad (2)$$

where $\eta_{j,i}$ and $\eta_{j,\mathbf{c}}$ represent the RF chain efficiency, $p^{\text{U2D}}_{j,i}[t]$ and $p^{\text{U2C}}_{j,\mathbf{c}}[t]$ are the transmission power for U2D and U2C communication, Δ^{U2D}_t and Δ^{U2C}_t denote the transmission duration for U2D and U2C communication, while $\zeta_{j,i}[t]$ and $\zeta_{j,\mathbf{c}}[t]$ capture the environmental effects influencing communication

energy consumption, such as atmospheric attenuation, channel fading, and interference. To incorporate environmental variability, $\zeta_{j,i}[t]$ and $\zeta_{j,\mathbf{c}}[t]$ can be explicitly defined as

$$\zeta_{j,i}[t] = \frac{1}{\mathbf{g}_{j,i}[t]h_{j,i}[t]}, \quad \zeta_{j,\mathbf{c}}[t] = \frac{1}{\mathbf{g}_{j,\mathbf{c}}[t]h_{j,\mathbf{c}}[t]}, \tag{3}$$

where $\mathbf{g}_{j,i}[t]$ and $\mathbf{g}_{j,\mathbf{c}}[t]$ represents the atmospheric attenuation factor, which depends on conditions such as humidity, temperature, and air pressure.

In addition to communication energy, the UAVs expend significant energy for propulsion, which depends on their velocity during flight as well as environmental factors. The energy required for propulsion at time t is formulated as:

$$\begin{aligned}\mathrm{Er}_j^f[t] =& \kappa \left\|\mathbf{v}_{\text{uav}}^j[t]\right\|^2 + \lambda_a \left\|a_j[t]\right\|^2 \\ &+ \lambda_w \|w[t]\|^2, \quad \forall t \in \{1,\ldots,T\},\end{aligned} \tag{4}$$

where $a_j[t]$ is the UAV's acceleration vector capturing the energy required for speed changes or maneuvering, $w[t]$ is the wind vector accounting for the impact of environmental wind resistance, $\kappa = 0.5\mu_n\Delta_t$ with μ_n denoting the total mass of the UAV including its payload, and Δ_t being the time slot duration, λ_a and λ_w are proportionality constants reflecting the energy consumption contributions from acceleration and wind resistance, respectively. The total energy consumption of a UAV j is the sum of its communication and propulsion energy, expressed as $\mathrm{Er}_j^c[t] = \mathrm{Er}_j^s[t] + \mathrm{Er}_j^f[t]$, $\forall t \in \{1,\ldots,T\}$. For the laser transmitter, it is assumed to operate with a constant transmit power denoted by $p^{\mathbf{l}} > 0$. The UAV is modeled to harvest energy from the laser transmitter's link, ensuring continuous power supply during its operation. The received power at the UAV at time t is

$$\mathrm{R}_{j,\mathbf{l}}^s[t] = \Delta_t p^{\mathbf{l}} \frac{\mathrm{Ar}\cdot\Omega_{j,\mathbf{l}}}{\left(S + \mathbf{d}_{\text{uav}}^{j,\mathbf{l}}[t]\Delta\theta\right)^2} e^{-\alpha \mathbf{d}_{\text{uav}}^{j,\mathbf{l}}[t]}, \tag{5}$$

where $t \in \{1,\ldots,T\}$, S is the initial diameter of the laser beam at the transmitter, $\Omega_{j,\mathbf{l}}$ denotes the optical efficiency of the combined laser-based harvesting system $\mathbf{l}$ and UAV j, $\Delta\theta$ is the angular spread of the laser beam (measured in radians), Ar corresponds to the area of the collection lens at the UAV receiver, α is the attenuation coefficient of the medium (measured in m^{-1}), $\mathbf{d}_{\text{uav}}^{j,\mathbf{l}}[t]$ is the distance between $\mathbf{l}$ and j at time t. Specifically, the term $\mathrm{Ar}\cdot(S + \mathbf{d}_{\text{uav}}^{j,\mathbf{l}}[t]\Delta\theta)^{-2}$ reflects the geometric spread of the laser beam as a function of the distance $\mathbf{d}_{\text{uav}}^{j,\mathbf{l}}[t]$, capturing the relationship between laser intensity and beam divergence. To model the UAV's energy harvesting, a constant efficiency factor $\omega_{\text{Er}} \in (0,1)$ is introduced, representing the fraction of received laser energy converted into usable electrical energy. The harvested laser energy at time t is

$$\begin{aligned}\mathrm{Er}_j^h[t] &= \omega_{\text{Er}}\mathrm{R}_{j,\mathbf{l}}^s[t] \\ &= \frac{\Delta_t(\omega_{\text{Er}}\mathrm{Ar}\Omega_{j,\mathbf{l}})p^{\mathbf{l}}e^{-\alpha\mathbf{d}_{\text{uav}}^{j,\mathbf{l}}[t]}}{\left(S + \mathbf{d}_{\text{uav}}^{j,\mathbf{l}}[t]\Delta\theta\right)^2}, \quad \forall t \in \{1,\ldots,T\}.\end{aligned} \tag{6}$$

The attenuation coefficient α is assumed to be negligible ($\alpha \leq 10^{-5}\ \mathrm{m}^{-1}$) under clear-air optical transmission with a link distance $\mathbf{d}_{\text{uav}}^{j,\mathbf{l}}[t] \leq 1\ \mathrm{km}$. In this regime, $e^{-\alpha\mathbf{d}_{\text{uav}}^{j,\mathbf{l}}[t]} \approx 1 - \mathbf{d}_{\text{uav}}^{j,\mathbf{l}}[t]$, resulting in $< 0.5\%$ attenuation. Therefore, the dominant factor influencing $\mathrm{R}_{j,\mathbf{l}}^s[t]$ and $\mathrm{Er}_j^h[t]$ is the geometric term $(S + \mathbf{d}_{\text{uav}}^{j,\mathbf{l}}[t]\Delta\theta)^{-2}$, which characterizes the inverse-square law of beam divergence. Since the angular spread $\Delta\theta$ is typically very small, and the laser's transmit power $p^{\mathbf{l}}$ is relatively high, the decline in harvested energy $\mathrm{Er}_j^h[t]$ as the distance $\mathbf{d}_{\text{uav}}^{j,\mathbf{l}}[t]$ increases occurs at a much slower rate compared to RF energy harvesting scenarios. To ensure that the UAV j maintains sufficient battery levels, the following laser energy harvesting constraints are imposed:

$$\zeta_{\text{Er}} \leq \mathrm{Er}_j^{\text{init}} + \sum_{t=1}^{T}\mathrm{Er}_j^h[t] - \sum_{t=1}^{T}\mathrm{Er}_j^c[t] \leq \mathrm{Er}_j, \tag{7}$$

where $\mathrm{Er}_j^{\text{init}} \in [\zeta_{\text{Er}}, \mathrm{Er}_j]$ is the initial state of charge, Er_j represents the UAV's energy capacity, denoting the maximum storage capability of its battery. It is assumed that the UAV is fully charged at the start of its mission. Denote by ζ_{Er} a minimum energy threshold that must be maintained throughout the flight to ensure the UAV has sufficient reserves for emergencies. This constraint accounts for the balance between the harvested energy $\mathrm{Er}_j^h[t]$ and the energy consumed during operation $\mathrm{Er}_j^c[t]$.

To streamline the analysis and simplify the formulation of the energy harvesting constraint, an auxiliary variable $b_j^{\text{aux}}[t]$ is introduced to enable a generalized representation of energy harvesting that is independent of the specific UAV trajectory, satisfying the conditions $b_j^{\text{aux}}[t] \geq \|\mathbf{q}_{\text{uav}}^j[t] - \mathbf{p}^{\mathbf{l}}\|^2 + H^2$, where $b_j^{\text{aux}}[t]$ is the squared distance between the UAV and the laser transmitter at time t. Using this auxiliary variable, the cumulative harvested energy up to time T is expressed as:

$$\begin{aligned}\mathrm{F}_j^{\text{cu}}\left(b_j^{\text{aux}}\right) =& \mathrm{Er}_j^h[t] \\ =& \sum_{t=1}^{T}\frac{\Delta_t(\omega_{\text{Er}}\mathrm{Ar}\Omega_{j,\mathbf{l}})p^{\mathbf{l}}e^{-\alpha\sqrt{b_j^{\text{aux}}[t]}}}{(S + \sqrt{b_j^{\text{aux}}[t]}\Delta\theta)^2}.\end{aligned} \tag{8}$$

Similarly, to streamline the notation for the energy consumption, another auxiliary variable $\mathrm{G}_j^{\text{cu}}(\mathbf{q}_{\text{uav}}^j) = \sum_{t=1}^{T}\mathrm{Er}_j^c[t]$.

C. Federated Learning Model

In the FL network, each network node $m \in \mathbf{S}_{\mathbf{all}}$[1], is associated with a local dataset $\mathcal{D}_m$. Denote by $c(\mathcal{D}_m)$ the number of elements in $\mathcal{D}_m$. The loss incurred by a model parameter vector $\boldsymbol{v}_m \in \mathbb{R}^{1\times\mathcal{E}}$ on a data sample $\mathbf{s}_m$ is denoted as $f_m(\boldsymbol{v}_m, \mathbf{s}_m)$, where $\mathcal{E}$ specifies the dimension of the model parameters. The local loss function at network node m is formulated as:

$$\mathcal{L}_m\left(\boldsymbol{v}_m; \mathcal{D}_m\right) = \frac{1}{c(\mathcal{D}_m)}\sum_{\mathbf{s}_m\in\mathcal{D}_m} f_m(\boldsymbol{v}_m, \mathbf{s}_m), \tag{9}$$

representing the average loss over the dataset $\mathcal{D}_m$. The primary objective of FL is to minimize the global loss function by determining the optimal parameter vector $\boldsymbol{v}^* \in \mathbb{R}^{1\times\mathcal{E}}$. The

[1]To refer to an arbitrary network node without committing to its type, we use the generic index $m \in \mathbf{S}_{\mathbf{all}}$ drawn from the union set $\mathbf{S}_{\mathbf{all}} \triangleq \mathbf{D} \cup \mathbf{C}$. This convention is used to represent FL data transmission between any two nodes through ordered pairs (m, n), where $m \neq n$. Specifically, not both nodes are IoT devices, $\neg(m \in \mathbf{D} \wedge n \in \mathbf{D})$. For link-level quantities, we denote a successful transmission from m to n at time t as $\varphi_{m,n}(t)$, with the corresponding probability $\mathrm{P}_{m,n}^{\text{suc}}$. In contrast, when discussing a specific communication link, we use i to refer to IoT devices and j to refer to UAVs.

global loss function is defined as the average of the local loss functions across all devices:

$$\boldsymbol{v}_m^* \triangleq \arg\min_{\boldsymbol{v}\in\mathbb{R}^{1\times K}} \frac{1}{c(\mathbf{S_{all}})} \sum_{m=1}^{c(\mathbf{S_{all}})} \mathcal{L}_m\left(\boldsymbol{v}_m; \mathcal{D}_m\right). \tag{10}$$

In this work, the FL process operates in two main stages: local training on devices and global aggregation at the central server.

1) Local Training Phase: Each device m refines its local model parameters by minimizing its local loss function $\mathcal{L}_m\left(\boldsymbol{v}_m; \mathcal{D}_m\right)$. The local parameter updates are performed iteratively over maximum K steps. Devices rely on stochastic gradient approximations $g_m(\boldsymbol{v}_m)$. At the k-th local iteration, the parameters of device m are updated with $\boldsymbol{v}_m^{(t,k+1)} = \boldsymbol{v}_m^{(t,k)} - \zeta_t g_m(\boldsymbol{v}_m^{(t,k)})$, where $\boldsymbol{v}_m^{(t,k)}$ is the local model parameters of node m at time t of the k-th iteration, and ζ_t is the learning rate at time t. In the considered scenarios, the learning rate, ζ_t, must adapt to additional factors such as device heterogeneity, communication variability, and resource constraints, as

$$\zeta_t = \frac{\zeta_0}{\sqrt{\frac{1}{c(\mathbf{S_{all}})}\sum_{m=1}^{c(\mathbf{S_{all}})} \frac{\mathrm{Er}_m}{\mathrm{Er}_{\max}}(\|g_m(\boldsymbol{v}_m^{(t,k)})\|^2 - \mu_g^2) + \lambda}}, \tag{11}$$

where ζ_0 is the initial learning rate, λ is a small positive constant used to prevent division by zero, $[\frac{1}{c(\mathbf{S_{all}})}\sum_{m=1}^{c(\mathbf{S_{all}})}(\|g_m(\boldsymbol{v}_m^{(t,k)})\|^2)]^{1/2}$ accounts for the magnitude of gradients across all devices, introducing adaptivity to the learning rate based on the gradient variability. In FL, devices often have non-IID data, causing significant gradient variability. We introduce the term $\mu_g = \frac{1}{c(\mathbf{S_{all}})}\sum_{m=1}^{c(\mathbf{S_{all}})}\|g_m(\boldsymbol{v}_m^{(t,k)})\|$ to adress this, which is the mean gradient magnitude across all devices. This modification accounts for the gradient variance, which reflects data heterogeneity across devices. A higher variance results in a lower learning rate to ensure stable convergence. In addition, energy constraints are another critical consideration for edge devices in federated learning. The term Er_m is the available energy at device m and $\mathrm{Er}_{\max}$ is the maximum energy budget across all devices. Thus, Eq. (11) ensures that the learning rate dynamically adjusts to device-level variability, communication constraints, and energy availability, enabling robust and efficient federated learning in real-world environments. Note that at the beginning of each communication round, the global model $\boldsymbol{v}^{(t)}$ is broadcast by the central server to all devices. The local models are initialized using the global model, such that $\boldsymbol{v}_m^{(t,0)} = \boldsymbol{v}^{(t)}$. Devices then perform K local iterations based on their data, resulting in updated local parameters $\boldsymbol{v}_m^{(t,\mathrm{K})}$, which are subsequently transmitted back to the central server.

2) Global Aggregation Phase: Following the local training phase, the CS aggregates the updated parameters received from all devices to compute the global model for the next communication round. The aggregation is typically performed using a weighted averaging scheme, where the contribution of each device depends on the size of its local dataset. A generalized global model at time $t+1$ can be expressed as

$$\boldsymbol{v}^{(t+1)} = \frac{1}{c(\mathbf{S_{all}})} \sum_{m=1}^{c(\mathbf{S_{all}})} \frac{c(\mathcal{D}_m)}{\sum_{m=1}^{c(\mathbf{S_{all}})} c(\mathcal{D}_m)} \boldsymbol{v}_m^{(t,\mathrm{K})}, \tag{12}$$

where $\sum_{m=1}^{c(\mathbf{S_{all}})} c(\mathcal{D}_m)$ is the total number of data samples across all devices. This aggregation ensures that devices with larger datasets have a proportionally higher impact on the global model, maintaining fairness in the federated learning process. The IoT devices and UAVs engage in bidirectional local cooperative updates through D2U and U2D communication. This mechanism ensures that local updates are refined collaboratively at both the IoT device and UAV levels before contributing to the global model, thereby enhancing robustness even under unreliable communication conditions. After completing K local training iterations, each node $m \in \mathbf{S_{all}}$ computes the local update $\Delta\boldsymbol{v}_m^{t+1}$, which represents the difference between its locally trained model parameters and the global model parameters received at the beginning of the round. Since environmental factors such as non-IID data distributions, communication reliability, and energy constraints vary across devices, the local update is

$$\begin{aligned}\Delta\boldsymbol{v}_m^{t+1} = &\frac{1}{\mathrm{K}}\sum_{k=1}^{\mathrm{K}}\Big[(\frac{\mathrm{Er}_m}{\mathrm{Er}_{\max}} - \zeta_t)\nabla\mathcal{L}_m(\boldsymbol{v}_m^{(t,k)}; \mathcal{D}_m) \\ &+\beta_m^{(t,k)}(\boldsymbol{v}_m^{(t,\mathrm{K})} - \boldsymbol{v}^{(t)})\Big],\end{aligned} \tag{13}$$

where the term $\nabla\mathcal{L}_m(\boldsymbol{v}_m^{(t,k)}; \mathcal{D}_m)$ is a modified gradient descent step, that the gradient is scaled by the learning rate ζ_t and the energy adjustmnt factor $\frac{\mathrm{Er}_m}{\mathrm{Er}_{\max}}$, and $\beta_m^{(t,k)}$ is a communication reliability factor, $\boldsymbol{v}_m^{(t,\mathrm{K})} - \boldsymbol{v}^{(t)}$ is a regularization term addressing gradient divergence that ensures that the local model remains aligned with the global model, preventing divergence in heterogeneous environments. The success of a transmission from node $m \in \mathbf{S_{all}}$ to node $n \in \mathbf{S_{all}}$ is modeled as $\varphi_{m,n}(t)$, where not two nodes are IoT devices $\neg(m \in \mathbf{D} \wedge n \in \mathbf{D})$. And we set $\varphi_{m,n}(t) = 1$ if $m = n$. Following the completion of bidirectional transmissions, each node m aggregates the updates that it receives from other nodes n. The aggregated update for node m is:

$$\Delta\tilde{\boldsymbol{v}}_m^t = \sum_{n\in\mathbf{S_{all}}} \varphi_{n,m}(t)\psi_{m,n}\Delta\boldsymbol{v}_n^t, \tag{14}$$

where $\psi_{m,n}$ represents the weight assigned by node m to the update received from node n. These weights ensure that the aggregated update reflects the contributions of all connected nodes, taking into account their relative importance or reliability. By aggregating updates from other nodes, each node m enhances the quality of its local model refinement, even in the presence of limited connectivity or transmission failures. The CS aggregates updates from all network nodes and refreshes the global model using a weighted sum:

$$\boldsymbol{v}^{(t)} = \boldsymbol{v}^{(t-1)} + \frac{1}{c(\mathbf{S_{all}})} \sum_{m\in\mathbf{S_{all}}} \mathbb{D}(m)\varphi_{m,c}(t)\Delta\tilde{\boldsymbol{v}}_m^t, \tag{15}$$

where $\mathbb{D}(m) = \frac{c(\mathcal{D}_m)\cdot\mathrm{Er}_m}{\sum_{n=1}^{c(\mathbf{S_{all}})} c(\mathcal{D}_n)\sum_{n=1}^{c(\mathbf{S_{all}})}\mathrm{Er}_n}$ is a normalized contribution weight for device m in the global aggregation process, which accounts for both the dataset's contribution and the energy metric for the device, $\varphi_{m,\mathbf{c}}(t) = 1$ indicates a successful transmission from node m to the CS, and $\varphi_{m,\mathbf{c}}(t) = 0$ indicates a failure transmission. In FL systems with UAV cooperative communication, the reliability of both D2U and U2S links can vary significantly, leading to potential biases

in the global aggregation process. Uneven communication success rates between devices or UAVs introduce discrepancies in the contributions to the global model, which can compromise fairness. To mitigate this bias and ensure fairness, the global aggregation must remain unbiased. Suppose that the local models of all devices converge to an optimal global model $\boldsymbol{v}^*$. Let $\mathbf{p}_1 \triangleq (\mathrm{P}^{\mathrm{suc}}_{m,\mathbf{c}})_{m\in\mathbf{S_{all}}}$ be the success probability from node m to the server $\mathbf{c}$, which specializes to $\mathrm{P}^{\mathrm{suc}}_{i,\mathbf{c}}$ for D2C link when $m = i$ and $\mathrm{P}^{\mathrm{suc}}_{j,\mathbf{c}}$ for U2C link when $m = j$. Likewise, $\mathbf{p}_2 \triangleq (\mathrm{P}^{\mathrm{suc}}_{m,n})_{m,n\in\mathbf{S_{all}}}$ denotes the success probability between any two nodes, where $\neg(m \in \mathbf{D} \wedge n \in \mathbf{D})$, specializing to $\mathrm{P}^{\mathrm{suc}}_{i,j}$ for D2U and $\mathrm{P}^{\mathrm{suc}}_{j,i}$ for U2D. Further set $(\mathrm{P}^{\mathrm{suc}}_{m,n})_{m,n\in\mathbf{S_{all}},m=n} = 1$ to reflect that self-transmission always succeeds with probability 1. Let $\boldsymbol{\Psi} \triangleq (\psi_{m,n})_{m,n\in\mathbf{S_{all}}}$ denote the weights assigned to the aggregated updates from devices and UAVs. And we set $\psi_{m,n} = 1$, if $m = n$.

Lemma 1. *For every $m \in \mathbf{S_{all}}$ and $t \geq 0$, a sufficient condition for unbiased aggregation is that the weights $\psi_{m,n}$ satisfy the following:*

$$\begin{aligned}&\mathbf{E}[\sum_{n\in\mathbf{S_{all}}} \varphi_{n,\mathbf{c}}(t)\varphi_{m,n}(t)\psi_{m,n}] \\ =&\mathrm{P}^{\mathrm{suc}}_{m,\mathbf{c}}\psi_{m,\mathbf{c}} + \sum_{n\in\mathbf{S_{all}}} \mathrm{P}^{\mathrm{suc}}_{n,\mathbf{c}}\mathrm{P}^{\mathrm{suc}}_{m,n}\psi_{m,n} = 1.\end{aligned} \tag{16}$$

Proof. We aim to ensure that the expected contribution of device m to the global model remains unbiased, which can be expressed as:

$$\frac{\mathbf{E}\left[\sum_{n\in\mathbf{S_{all}}}\varphi_{n,\mathbf{c}}(t)\varphi_{m,n}(t)\psi_{m,n}\Delta\boldsymbol{v}^t_m \,|\, \Delta\boldsymbol{v}^t_m\right]}{c(\mathbf{S_{all}})} = \frac{\Delta\boldsymbol{v}^t_m}{c(\mathbf{S_{all}})}. \tag{17}$$

Since the random variables $\varphi_{n,\mathbf{c}}(t)$ and $\varphi_{m,n}(t)$ are statistically independent of $\Delta\boldsymbol{v}^t_m$, the expectation simplifies to:

$$\mathbf{E}\left[\sum_{n\in\mathbf{S_{all}}} \varphi_{n,\mathbf{c}}(t)\varphi_{m,n}(t)\psi_{m,n}\right]\Delta\boldsymbol{v}^{t+1}_m. \tag{18}$$

For this equality to hold, the sum of the expected weights and communication success probabilities must satisfy the unbiased aggregation condition, thereby substituting the sucess probability and reducing to:

$$\mathrm{P}^{\mathrm{suc}}_{m,\mathbf{c}}\psi_{m,\mathbf{c}} + \sum_{n\in\mathbf{S_{all}}} \mathrm{P}^{\mathrm{suc}}_{n,\mathbf{c}}\mathrm{P}^{\mathrm{suc}}_{m,n}\psi_{m,n} = 1, \tag{19}$$

which confirms that the weights $\psi_{m,n}$ must be carefully designed to balance the influence of direct and cooperative transmissions, ensuring that devices with different communication reliabilities contribute fairly to the global model. This unbiased aggregation guarantees that the federated learning system remains robust and fair despite uneven communication success rates. □

To establish the theoretical foundation of the considered FL system, we introduce the following assumptions:

Assumption 1: The local loss functions $\mathcal{L}_m(\boldsymbol{v})$ are L-smooth, meaning their gradients satisfy Lipschitz continuity $\|\nabla\mathcal{L}_m(\boldsymbol{v}) - \nabla\mathcal{L}_m(\boldsymbol{v}')\| \leq L\|\boldsymbol{v} - \boldsymbol{v}'\|$, for all $\boldsymbol{v}, \boldsymbol{v}' \in \mathbb{R}^{1\times K}$ and $m \in \mathbf{S_{all}}$, where L is the smoothness constant.

Assumption 2: The stochastic gradients $g_m(\boldsymbol{v})$, for all $m \in \mathbf{S_{all}}$ and $\boldsymbol{v} \in \mathbb{R}^{1\times K}$, computed by each device are unbiased estimators of the true gradients with a bounded variance, which holds that $\mathbf{E}[g_m(\boldsymbol{v})] = \nabla\mathcal{L}_m(\boldsymbol{v})$ and the variance of the stochastic gradients is bounded by a constant ϑ^2 such that $\mathbf{E}[\|g_m(\boldsymbol{v}) - \nabla\mathcal{L}_m(\boldsymbol{v})\|^2] \leq \vartheta^2$.

Assumption 3: The local loss functions $\mathcal{L}_m(\boldsymbol{v})$ are assumed to be μ-strongly convex. For every device $m \in \mathbf{S_{all}}$ and for all $\boldsymbol{v}, \boldsymbol{v}' \in \mathbb{R}^{1\times K}$, the following inequality holds $\langle\nabla\mathcal{L}_m(\boldsymbol{v}) - \nabla\mathcal{L}_m(\boldsymbol{v}'), \boldsymbol{v} - \boldsymbol{v}'\rangle \geq \mu\|\boldsymbol{v} - \boldsymbol{v}'\|^2$, where $\mu > 0$ is the strong convexity constant.

Assumption 4: The weights $\psi_{m,n}$, for all $m, n \in \mathbf{S_{all}}$, assigned to the updates from neighboring devices are non-negative, which satisfy $\psi_{m,n} \geq 0$.

Lemma 2. *For every $t \geq t_0$, the upper bound of $\mathbf{E}\|\boldsymbol{v}^{(t+1)} - \boldsymbol{v}^*\|^2$ can be expressed as:*

$$\begin{aligned}\mathbf{E}\|\boldsymbol{v}^{(t+1)} - \boldsymbol{v}^*\|^2 \leq& \frac{(t_0\mathrm{K}+1)}{(t\mathrm{K}+1)^2}\|\boldsymbol{v}^{(0)} - \boldsymbol{v}^*\|^2 \\ &+ \mathcal{B}_1\frac{(\mathrm{K}-1)^2}{t\mathrm{K}+1} + \mathcal{B}_2(\mathbf{p}_1,\mathbf{p}_2,\boldsymbol{\Psi})\frac{\mathrm{K}}{t\mathrm{K}+1} \\ &+ \mathcal{B}_3(\mathbf{p}_1,\mathbf{p}_2,\boldsymbol{\Psi})\frac{\mathrm{K}-1}{(t\mathrm{K}+1)^2},\end{aligned} \tag{20}$$

where:

$$t_0 \triangleq \max\{\frac{L}{\mu}, 4(\frac{2L^2\mathcal{Z}(\mathbf{p}_1,\mathbf{p}_2,\boldsymbol{\Psi})}{\mu^2 c(\mathbf{S_{all}})^2} + 1), \frac{1}{\mathrm{K}}, \frac{4c(\mathbf{S_{all}})}{\mu^2\ \mathrm{K}}\}, \tag{21}$$

and the terms $\mathcal{B}_1, \mathcal{B}_2(\mathbf{p}_1,\mathbf{p}_2,\boldsymbol{\Psi})$, and $\mathcal{B}_3(\mathbf{p}_1,\mathbf{p}_2,\boldsymbol{\Psi})$ are defined as:

$$\mathcal{B}_1 \triangleq \frac{16\vartheta^2}{\mu^2 c(\mathbf{S_{all}})}L^2 e \tag{22}$$

$$\mathcal{B}_2(\mathbf{p}_1,\mathbf{p}_2,\boldsymbol{\Psi}) \triangleq \frac{32\vartheta^2}{\mu^2 c(\mathbf{S_{all}})^2}\mathcal{Z}(\mathbf{p}_1,\mathbf{p}_2,\boldsymbol{\Psi}) \tag{23}$$

$$\mathcal{B}_3(\mathbf{p}_1,\mathbf{p}_2,\boldsymbol{\Psi}) \triangleq \frac{256\vartheta^2}{\mu^4}L^2 e(1 + \frac{2}{c(\mathbf{S_{all}})^2}\mathcal{Z}(\mathbf{p}_1,\mathbf{p}_2,\boldsymbol{\Psi})), \tag{24}$$

and $\mathcal{Z}(\mathbf{p}_1,\mathbf{p}_2,\boldsymbol{\Psi})$ is given by:

$$\begin{aligned}&\mathcal{Z}(\mathbf{p}_1,\mathbf{p}_2,\boldsymbol{\Psi}) \\ &\triangleq \sum_{m,n,k\in\mathbf{S_{all}}} \mathrm{P}^{\mathrm{suc}}_{n,\mathbf{c}}\left(1 - \mathrm{P}^{\mathrm{suc}}_{n,\mathbf{c}}\right)\mathrm{P}^{\mathrm{suc}}_{m,n}\mathrm{P}^{\mathrm{suc}}_{k,n}\psi_{m,n}\psi_{n,k} \\ &+ \sum_{m,n\in\mathbf{S_{all}}} \mathrm{P}^{\mathrm{suc}}_{n,\mathbf{c}}\mathrm{P}^{\mathrm{suc}}_{m,n}\left(1 - \mathrm{P}^{\mathrm{suc}}_{m,n}\right)\psi^2_{m,n} \\ &+ \sum_{m,k\in\mathbf{S_{all}}} \mathrm{P}^{\mathrm{suc}}_{m,\mathbf{c}}\mathrm{P}^{\mathrm{suc}}_{k,\mathbf{c}}\left(\mathbf{E}_{m,k} - \mathrm{P}^{\mathrm{suc}}_{m,k}\mathrm{P}^{\mathrm{suc}}_{k,m}\right)\psi_{m,k}\psi_{k,m}.\end{aligned} \tag{25}$$

Proof. Please refer to Appendix A[2]. □

Based on **Lemma 2**, the expected distance between the global model $\boldsymbol{v}^{(t+1)}$ and the optimal global model $\boldsymbol{v}^*$ is predominantly influenced by the term $\mathcal{Z}(\mathbf{p}_1,\mathbf{p}_2,\boldsymbol{\Psi})$. This term reflects the combined effects of the transmission success probabilities of D2U, U2S, and D2S links, as well as the local update weights $\boldsymbol{\Psi}$. Specifically, $\mathcal{Z}(\mathbf{p}_1,\mathbf{p}_2,\boldsymbol{\Psi})$ quantifies how communication reliability and weight allocations impact the aggregation process and convergence performance. In this

[2]The node k is chosen from all nodes except m and n, denoted as $k \in \mathbf{S_{all}} \setminus \{m,n\}$. No pair among them are both IoT devices, denoted as $|\{x \in \{m,n,k\} : x \in \mathbf{D}\}| \leq 1$.

context, the D2C success probabilities $\mathrm{P}^{\mathrm{suc}}_{j,\mathbf{c}}$ are assumed to be fixed and known, while for simplicity, the U2D success probabilities are considered equivalent to the D2U success probabilities $\mathrm{P}^{\mathrm{suc}}_{i,j}$. In addition, $\mathcal{Z}(\mathbf{p}_1, \mathbf{p}_2, \mathbf{\Psi})$ represents the only term in the classical FedAvg bound that cannot be directly controlled. This quantity increases when communication links exhibit unreliability or when weights Ψ are significantly imbalanced. Conversely, it is reduced when communication-layer optimization improves either factor. The convergence gap can be proportionally decreased with each percentage improvement in end-to-end success probability.

The objective is to minimize $\mathcal{Z}\left(\mathbf{p}_1, \mathbf{p}_2, \mathbf{\Psi}\right)$[3] to tighten the upper bound of the distance described in Eq. (20), which aims to improve the performance of the global aggregation process by reducing the variance introduced by communication reliability and aggregation weights. Achieving this goal requires optimizing the transmission probabilities $\mathrm{P}^{\mathrm{suc}}_{i,j}$ and $\mathrm{P}^{\mathrm{suc}}_{j,\mathbf{c}}$, as well as the local update weights $\mathbf{\Psi}$, for each node. Since the successful transmission probabilities for both D2U and U2C links are influenced by blocklength allocation and UAV trajectory, these parameters must also be optimized. To address these dependencies, we define $\boldsymbol{l}^{\mathrm{U2C}} \triangleq (l_j)_{j\in\mathbf{U}}$ as the blocklengths for U2C links, $\boldsymbol{l}^{\mathrm{D2U}} \triangleq (l_{i,j})_{i\in\mathbf{D},j\in\mathbf{U}}$ as the blocklengths for D2U links, $\boldsymbol{b}^{\mathrm{aux}} \triangleq (b^{\mathrm{aux}}_j)_{j\in\mathbf{U}}$ as auxiliary variables, and $\mathbf{q}_{\mathrm{uav}} \triangleq (\mathbf{q}^j_{\mathrm{uav}})_{j\in\mathbf{U}}$ as the UAV trajectory across all communication rounds. For time instant $t \in \{1, \ldots, T\}$, the optimization problem can be formally expressed as minimizing $\mathcal{Z}\left(\mathbf{p}_1, \mathbf{p}_2, \mathbf{\Psi}\right)$ by jointly optimizing $\boldsymbol{l}^{\mathrm{U2C}}, \boldsymbol{l}^{\mathrm{D2U}}, \mathbf{q}_{\mathrm{uav}}, \mathbf{\Psi}$, and transmission powers $p_{j,c}$ and $p_{i,j}$, which can be expressed as

$$\min_{\boldsymbol{l}^{\mathrm{U2C}}, \boldsymbol{l}^{\mathrm{D2U}}, \mathbf{q}_{\mathrm{uav}}, b^{\mathrm{aux}}, \mathbf{\Psi}} \mathcal{Z}\left(\mathbf{p}_1, \mathbf{p}_2, \mathbf{\Psi}\right)$$

$$\text{s.t.} \quad \zeta_{\mathrm{Er}} \leq \mathrm{Er}^{init}_j + \mathrm{F}^{\mathrm{cu}}_j\left(b^{\mathrm{aux}}_j\right) - \mathrm{G}^{\mathrm{cu}}_j\left(\mathbf{q}^j_{\mathrm{uav}}\right) \leq \mathrm{Er}_j, \quad (26a)$$

$$\left\|\mathbf{q}^j_{\mathrm{uav}}[t] - \mathbf{p}^{\mathbf{c}}\right\|^2 + H^2 \leq b^{\mathrm{aux}}_j\,[t], \quad (26b)$$

$$\left\|\mathbf{q}^j_{\mathrm{uav}}\,[t+1] - \mathbf{q}^j_{\mathrm{uav}}\,[t]\right\| \leq V_{\max}\Delta_t, \quad (26c)$$

$$\mathbf{q}^j_{\mathrm{uav}}\,[1] = \mathbf{q}^{j,I}_{\mathrm{uav}}, \quad \mathbf{q}^j_{\mathrm{uav}}[T] = \mathbf{q}^{j,F}_{\mathrm{uav}}, \quad (26d)$$

$$l^{\mathrm{D2U}}_{i,j}[t] + l^{\mathrm{U2C}}_{j,\mathbf{c}}[t] \leq M_{\mathrm{tot}}\,, \quad \forall (i,j) \in \mathcal{P}, \quad (26e)$$

$$\epsilon_{i,j}[t] \leq \epsilon^{\max}_{i,j}, \quad \epsilon_{j,\mathbf{c}}[t] \leq \epsilon^{\max}_{j,\mathbf{c}}, \quad \forall (i,j) \in \mathcal{P}, \quad (26f)$$

$$p^{\mathrm{D2U}}_{i,j}[t] \geq 0, \quad p^{\mathrm{U2C}}_{j,\mathbf{c}}[t] \geq 0, \quad \forall (i,j) \in \mathcal{P}, \quad (26g)$$

$$l^{\mathrm{D2U}}_{i,j}[t], l^{\mathrm{U2C}}_{j,\mathbf{c}}[t] \in \mathbb{Z}, \quad \forall (i,j) \in \mathcal{P}, \quad (26h)$$

$$\sum_{j\in\mathbf{U}} \mathrm{P}^{\mathrm{suc}}_{j,\mathbf{c}} \cdot \mathrm{P}^{\mathrm{suc}}_{i,j} \cdot \psi_{j,i} = 1, \quad \psi_{j,i} \geq 0, \quad (26i)$$

$$j \in \mathbf{U}, i \in \mathbf{D}, (i,j) \in \mathcal{P}. \quad (26j)$$

The constraints are designed to ensure energy efficiency, trajectory feasibility, communication reliability, and resource allocation within the system. The energy constraints enforce that the residual energy ζ_{Er} of a UAV at any time t lies within an acceptable range defined by the auxiliary energy function $\mathrm{Er}_j + \mathrm{F}^{\mathrm{cu}}_j(b^{\mathrm{aux}}_j) - \mathrm{G}^{\mathrm{cu}}_j(\mathbf{q}^j_{\mathrm{uav}}) \leq \mathrm{Er}_j$, for each UAV $j \in \mathbf{U}$. The trajectory constraints ensure that the position of the UAV $\mathbf{q}^j_{\mathrm{uav}}[t]$ lies within a feasible range relative to the center position $\mathbf{p}^{\mathbf{c}}$, bounded by $\|\mathbf{q}^j_{\mathrm{uav}}\,[t] - \mathbf{p}^{\mathbf{c}}\|^2 + H^2 \leq b^{\mathrm{aux}}_j\,[t]$. Furthermore, the UAV's maximum velocity is constrained by $\|\mathbf{q}^j_{\mathrm{uav}}\,[t+1] - \mathbf{q}^j_{\mathrm{uav}}\,[t]\| \leq V_{\max}\Delta_t$, ensuring that the UAV adheres to its physical motion limitations. The UAV's initial and final positions are fixed, denoted by $\mathbf{q}^j_{\mathrm{uav}}\,[1] = \mathbf{q}^{j,I}_{\mathrm{uav}}$ and $\mathbf{q}^j_{\mathrm{uav}}\,[T] = \mathbf{q}^{j,F}_{\mathrm{uav}}$, respectively. Communication constraints guarantee that the allocated uplink $\boldsymbol{l}^{\mathrm{U2C}}$ and downlink $\boldsymbol{l}^{\mathrm{D2U}}$ blocklengths do not exceed the total system blocklength budget, $l^{\mathrm{D2U}}_{i,j}[t] + l^{\mathrm{U2C}}_{j,\mathbf{c}}[t] \leq M_{\mathrm{tot}}$, for any device-UAV pair $(i,j) \in \mathcal{P}$. Packet error probabilities are bounded to ensure communication reliability, with $\epsilon_{i,j}[t] \leq \epsilon^{\max}_{i,j}$ and $\epsilon_{j,\mathbf{c}}[t] \leq \epsilon^{\max}_{j,\mathbf{c}}$. Transmission powers for both D2U $p_{i,j}[t]$ and U2C $p_{j,\mathbf{c}}[t]$ links must remain non-negative, with $p_{i,j}[t] \geq 0$ and $p_{j,\mathbf{c}}[t] \geq 0$. Blocklength variables $l^{\mathrm{D2U}}_{i,j}[t]$ and $l^{\mathrm{U2C}}_{j,\mathbf{c}}[t]$ are constrained to integer values to reflect practical communication system constraints. Finally, the aggregation weight constraints ensure unbiased global model updates. These weights, $\psi_{j,i}$, must satisfy $\sum_{j\in\mathbf{U}} \mathrm{P}^{\mathrm{suc}}_{j,\mathbf{c}}\,\mathrm{P}^{\mathrm{suc}}_{i,j}\,\psi_{j,i} = 1$ and must remain non-negative, $\psi_{j,i} \geq 0$, for all devices $i \in \mathbf{D}$. This guarantees that the aggregation process accounts for stochastic communication success probabilities and preserves fairness across all devices in the federated learning system.

IV. The Proposed CCLO Scheme

The proposed CCLO scheme is developed to optimize the FL in UAV-assisted systems by integrating three blocks: dynamic blocklength optimization, UAV trajectory optimization and local update weight adjustment. First, we focus on determining the optimal communication blocklengths based on the device position constraints and specific energy requirements, which ensures efficient and reliable data transmission with minimal latency. Second, in the UAV trajectory optimization block, we optimize the UAV's movement to reduce transmission distances and maximize coverage for devices. The IID properties of local data can be impoved, facilitating the faster convergence of the global model. Third, the local model updates are fine-tuned by dynamically adjusting the weights according to communication reliability and the quality of local data collected by each device. Specifically, by leveraging UAVs for data collection and sharing, the scheme ensures that local models from different devices become more aligned, accelerating the global model's convergence. The UAV facilitates the process of augmenting the IID properties between local datasets by actively collecting data from multiple devices and sharing it in a coordinated manner.

Thus, the proposed CCLO scheme decomposes the non-convex problem Eq. (26) into three iterative subproblems. The first subproblem focuses on optimizing the time-varying blocklengths $\boldsymbol{l}^{\mathrm{D2U}}$ and $\boldsymbol{l}^{\mathrm{U2C}}$, to maximize communication reliability and minimize latency in both the D2U and U2C communication phases. Next, UAV trajectory optimization optimizes the UAV trajectories $\mathbf{q}_{\mathrm{uav}}$, to ensure efficient spatial coverage and reduce communication distance, enhancing both

[3]The objective $\mathcal{Z}(\mathbf{p}_1, \mathbf{p}_2, \mathbf{\Psi})$ is written with generic node indices $m, n, k \in \mathcal{S}_{\mathrm{all}}$ to aggregate connection–probability and weighting effects over all possible node interactions, whereas the constraints are expressed with $i \in \mathbf{D}$ and $j \in \mathbf{U}$ because they bind type-specific physical variables—trajectory $\mathbf{q}^j_{\mathrm{uav}}$, energy and motion limits, blocklengths $l^{\mathrm{D2U}}_{i,j}, l^{\mathrm{U2C}}_{j,\mathbf{c}}$, powers $p^{\mathrm{D2U}}_{i,j}, p^{\mathrm{U2C}}_{j,\mathbf{c}}$, and error budgets $\epsilon_{i,j}, \epsilon_{j,\mathbf{c}}$—that only make sense for the corresponding network node. This is consistent since each generic index is realized as a concrete type when evaluated, and the probability terms $\mathrm{P}^{\mathrm{suc}}_{\{\cdot,\cdot\}}$ inside $\mathcal{Z}$ are functions of those constrained variables, specializing to $\mathrm{P}^{\mathrm{suc}}_{i,j}$ for D2U, $\mathrm{P}^{\mathrm{suc}}_{j,i}$ for U2D and $\mathrm{P}^{\mathrm{suc}}_{m,\mathbf{c}}$ for arbitrary nodes to server.

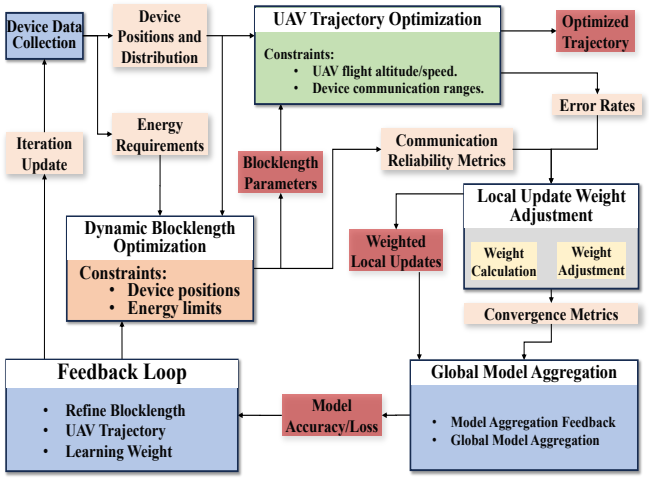

Fig. 2. Overview of the CCLO Scheme.

transmission efficiency and energy utilization. Lastly, the local update weight adjustment optimizes the local update weights $\mathbf{\Psi}$ to meet the unbiasedness constraint specified in condition Eq. (26i), ensuring fair aggregation of model updates across all devices in the network. Throughout these iterative optimization steps, the transmission powers $p_{i,j}^{\mathrm{D2U}}[t]$ and $p_{j,\mathbf{c}}^{\mathrm{U2C}}[t], \forall (i,j) \in \mathcal{P}$, for D2U and U2C communication links are treated as fixed parameters, simplifying the structure and allowing for efficient refinement. This decomposition approach not only addresses the non-convex nature of the problem but also provides a systematic framework that optimizes key components of the network, ensuring robust and reliable performance for federated learning in UAV-assisted systems.

A. Blocklength Optimization

Suppose $\mathrm{P}_{m,n}^{\mathrm{suc}} = \mathrm{P}_{n,m}^{\mathrm{suc}}$ for $\forall m,n \in \mathbf{S}_{\mathrm{all}}$. The Eq. (26) exhibits a separability property with respect to the communication success probabilities $\mathrm{P}_{n,\mathbf{c}}^{\mathrm{suc}}$ and $\mathrm{P}_{m,n}^{\mathrm{suc}}$ for $n \in \mathbf{U}$ and $m \in \mathbf{D}$, allowing the third term in the objective function of Eq. (26) to be reformulated as

$$\sum_{i\in\mathbf{D},k\in\mathbf{S}_{\mathrm{all}}} \mathrm{P}_{i,\mathbf{c}}^{\mathrm{suc}}\mathrm{P}_{k,\mathbf{c}}^{\mathrm{suc}}\mathrm{P}_{i,k}^{\mathrm{suc}}\left(1-\mathrm{P}_{i,k}^{\mathrm{suc}}\right)\psi_{i,k}\psi_{k,i}, \tag{27}$$

where $\neg(i \in \mathbf{D} \wedge k \in \mathbf{D})$. Using the property $\mathrm{P}_{j,\mathbf{c}}^{\mathrm{suc}}\mathrm{P}_{i,j}^{\mathrm{suc}}\left(1-\mathrm{P}_{i,j}^{\mathrm{suc}}\right) < \mathrm{P}_{j,\mathbf{c}}^{\mathrm{suc}}\mathrm{P}_{i,j}^{\mathrm{suc}}\left(1-\mathrm{P}_{j,\mathbf{c}}^{\mathrm{suc}}\mathrm{P}_{i,j}^{\mathrm{suc}}\right)$ for $\mathrm{P}_{j,\mathbf{c}}^{\mathrm{suc}}, \mathrm{P}_{i,j}^{\mathrm{suc}} \in (0,1)$, we extend the upper bound and reformulate Eq. (26) as follows:

$$\begin{aligned}\min_{\substack{\boldsymbol{l}^{\mathrm{U2C}},\boldsymbol{l}^{\mathrm{D2U}}\\ \mathbf{q}_{\mathrm{uav}},\boldsymbol{b}^{\mathrm{aux}}}} \quad & \sum_{i\in\mathbf{D}} \mathrm{P}_{j,\mathbf{c}}^{\mathrm{suc}}\mathrm{P}_{i,j}^{\mathrm{suc}}\left(1-\mathrm{P}_{j,\mathbf{c}}^{\mathrm{suc}}\mathrm{P}_{i,j}^{\mathrm{suc}}\right)\psi_{j,i}^2 \\ & + 2\sum_{k\in\mathbf{D}}\sum_{i\in\mathbf{D}} \mathrm{P}_{j,\mathbf{c}}^{\mathrm{suc}}\mathrm{P}_{i,j}^{\mathrm{suc}}\,\mathrm{P}_{j,k}^{\mathrm{suc}}\psi_{i,j}\psi_{j,k} \\ & + \sum_{i\in\mathbf{D}} \mathrm{P}_{i,\mathbf{c}}^{\mathrm{suc}}\mathrm{P}_{j,\mathbf{c}}^{\mathrm{suc}}\,\mathrm{P}_{i,j}^{\mathrm{suc}}\,\psi_{j,i}\psi_{i,j}, \\ \text{s.t.} \quad & (26a)-(26h).\end{aligned} \tag{28}$$

The three terms in the objective function demonstrate a monotonically decreasing behavior with respect to $\mathrm{P}_{j,\mathbf{c}}^{\mathrm{suc}}$ and $\mathrm{P}_{i,j}^{\mathrm{suc}}$ within the interval $[0.5, 1]$. In scenarios where high communication reliability is required, it is expected that both $\mathrm{P}_{j,\mathbf{c}}^{\mathrm{suc}}$ and $\mathrm{P}_{i,j}^{\mathrm{suc}}$ will exceed 0.5 , ensuring stable and effective communication across the system. Given this relationship, the optimization process aims to minimize the error probabilities $\epsilon_{j,\mathbf{c}}$ and $\epsilon_{i,j}$ for each communication link. The total packet error rate $\varepsilon_j[t]$ for the D2U and U2C transmission at time t for each device-UAV pair $(i,j) \in \mathbf{P}$ can be expressed as $\varepsilon_j[t] = \epsilon_{i,j}[t] + (1-\epsilon_{i,j}[t])\,\epsilon_{j,\mathbf{c}}[t]$. Given that the likelihood of simultaneous transmission errors, represented by $\epsilon_{i,j}[t]\epsilon_{j,\mathbf{c}}[t]$, approaches zero, this term becomes negligible. Therefore, the total packet error rate simplifies to $\varepsilon_j[t] = \epsilon_{i,j}[t] + \epsilon_{j,\mathbf{c}}[t]$. The objective is to determine the optimal time-varying blocklengths $l_{i,j}^{\mathrm{D2U}}[t]$ and $l_{j,\mathbf{c}}^{\mathrm{U2C}}[t]$ for each device-UAV pair and UAV-CS pair. For this optimization, the transmission powers $p_{i,j}[t]$ and $p_{j,\mathbf{c}}[t]$, as well as the UAV's trajectory $\mathbf{q}_{\mathrm{uav}}^{j}[t]$, are treated as fixed parameters. It is important to note that the blocklength variables are inherently integers, making the problem non-convex. To simplify, we relax the integer constraint by assuming that $l_{i,j}^{\mathrm{D2U}}[t]$ and $l_{j,\mathbf{c}}^{\mathrm{U2C}}[t]$ are continuous variables. With this relaxation, the problem in Eq. (28) is reformulated for each UAV $j \in \mathbf{U}$ as:

$$\begin{aligned}\min_{l_{j,\mathbf{c}}^{\mathrm{U2C}},l_{i,j}^{\mathrm{D2U}}} \quad & \frac{1}{T}\sum_{t=1}^{T}\varepsilon_j[t] \\ \text{s.t.} \quad & l_{i,j}^{\mathrm{D2U}}[t] \geq 0, \quad l_{j,\mathbf{c}}^{\mathrm{U2C}}[t] \geq 0, \quad \forall t \in \{1,\ldots,T\}, \\ & (26\mathrm{e})-(26\mathrm{f}).\end{aligned} \tag{29}$$

By adjusting the blocklengths $l_{i,j}^{\mathrm{D2U}}[t]$ and $l_{j,\mathbf{c}}^{\mathrm{U2C}}[t]$, the scheme optimizes the efficiency of data transmission, laying the foundation for subsequent UAV trajectory optimization and local update weight adjustment.

To establish the convexity of the objective function in problem Eq. (29), we note that $\epsilon_{i,j}[t]$ and $\epsilon_{j,\mathbf{c}}[t]$ exhibit analogous analytical structures, thereby permitting a focused convexity analysis on a representative term such as $\epsilon_{j,\mathbf{c}}[t]$. For an arbitrary iteration time instant t, we define the composite function $f(l_{j,\mathbf{c}}^{\mathrm{U2C}}[t]) = f(\gamma_{j,\mathbf{c}}^{*}[t], l_{j,\mathbf{c}}^{\mathrm{U2C}}[t])$. The first component of the objective function is formulated as:

$$\begin{aligned}\epsilon_{j,\mathbf{c}}[t] &= \mathbf{H}(f(l_{j,\mathbf{c}}^{\mathrm{U2C}}[t])) \\ &= \mathbf{H}\left(A_1\sqrt{l_{j,\mathbf{c}}^{\mathrm{U2C}}[t]}(B_1 - \frac{L}{l_{j,\mathbf{c}}^{\mathrm{U2C}}[t]})\right),\end{aligned} \tag{30}$$

where $A_1 = \frac{\ln(2)}{\sqrt{\Gamma(\gamma_{j,\mathbf{c}}^{*}[t])}}$ and $B_1 = \log_2(1+\gamma_{j,\mathbf{c}}^{*}[t])$ are time-dependent constants independent of $l_{j,\mathbf{c}}^{\mathrm{U2C}}[t]$. To assess convexity, we derive the second-order derivative of $l_{j,\mathbf{c}}^{\mathrm{U2C}}[t]$:

$$\frac{\partial^2 f\left(l_{j,\mathbf{c}}^{\mathrm{U2C}}[t]\right)}{\partial^2 l_{j,\mathbf{c}}^{\mathrm{U2C}}[t]} = -\frac{A_1\left(3L + B_1 l_{j,\mathbf{c}}^{\mathrm{U2C}}[t]\right)}{4\sqrt{(l_{j,\mathbf{c}}^{\mathrm{U2C}}[t])^5}}. \tag{31}$$

Given the positivity of $l_{j,\mathbf{c}}^{\mathrm{U2C}}[t], A_1, B_1$, and L, the second derivative is unambiguously negative, confirming the concavity of $f(l_{j,\mathbf{c}}^{\mathrm{U2C}}[t])$. Since $\mathbf{H}(a)$ is a convex and nonincreasing function for $a \geq 0$, the composition $\mathbf{H}(f(l_{j,\mathbf{c}}^{\mathrm{U2C}}[t]))$ inherits convexity through the concavity of $f(l_{j,\mathbf{c}}^{\mathrm{U2C}}[t])$. This result follows from the general principle that the composition of a convex nonincreasing function with a concave function yields a convex function, thereby solidifying the convexity of $\epsilon_{j,\mathbf{c}}[t]$ and, by structural analogy, $\epsilon_{i,j}[t]$.

To rigorously establish the convex optimization properties of Eq. (29), we extend the analytical framework through systematic notation alignment and enhanced mathematical exposition.

Following the convexity confirmation of $\epsilon_{j,\mathbf{c}}[t]$ derived earlier, the structural equivalence between $\epsilon_{i,j}[t]$ and $\epsilon_{j,\mathbf{c}}[t]$ permits analogous convexity-preserving operations. Specifically, the composite function $\mathbf{H}(f(l_{i,j}^{\mathrm{D2U}}[t]))$ governing $\epsilon_{i,j}[t]$ inherits convexity through identical derivative analysis, given that $l_{i,j}^{\mathrm{D2U}}[t]$ maintains positivity constraints equivalent to $l_{j,\mathbf{c}}^{\mathrm{U2C}}[t]$. Consequently, the aggregated objective function $\epsilon_{j,\mathbf{c}}[t]+\epsilon_{i,j}[t]$ preserves convexity through linear combination of convex components, while all operational constraints in Eq. (29) maintain their inherent convex characteristics. The critical reformulation of constraint Eq. (26a-26f) is achieved through inverse derivation of the minimum distance requirements for U2C and D2U links. By resolving the inequality $\mathbf{H}(f(l_{j,\mathbf{c}}^{\mathrm{U2C}}[t])) \leq \epsilon_{j,\mathbf{c}}^{\max}$ for $l_{j,\mathbf{c}}^{U2\mathrm{C}}[t]$, we derive the explicit lower bounds:

$$l_{j,\mathbf{c}}^{\mathrm{U2C}}[t] \geq L_1^b[t] = \frac{\epsilon_{j,\mathbf{c}}^{\max}\sqrt{4\ln(2)^2 A_1 L + 2\left(\epsilon_{j,\mathbf{c}}^{\max}\right)^2} + \left(\epsilon_{j,\mathbf{c}}^{\max}\right)^2}{2\ln(2)^2 A_1^2} + \frac{L}{2A_1}, \quad \forall t \in \{1,\ldots,T\}, \tag{32}$$

$$l_{i,j}^{\mathrm{D2U}}[t] \geq L_2^b[t] = \frac{\epsilon_{i,j}^{\max}\sqrt{4\ln(2)^2 A_2 L + 2\left(\epsilon_{i,j}^{\max}\right)^2} + \left(\epsilon_{i,j}^{\max}\right)^2}{2\ln(2)^2 A_2^2} + \frac{L}{2A_2}, \quad \forall t \in \{1,\ldots,T\}, \tag{33}$$

where $A_2 = \frac{\ln(2)}{\sqrt{\Gamma(\gamma_{i,j}^*[t])}}$ characterizes the D2U link adaptation parameter. This transformation rigorously demonstrates that constraint (26a) becomes operationally redundant, as the derived lower bounds $L_1^b[t]$ and $L_2^b[t]$ inherently enforce stricter spatial constraints than the original formulation. The convex program therefore reduces to optimizing over these analytically derived distance floors while maintaining all convexity guarantees essential for gradient-based solution techniques.

To address the convex optimization challenges inherent in problem Eq. (29), we first emphasize the temporal dependency of its constraints, which necessitates per-round optimization over the discrete time horizon $t \in \{1,\ldots,T\}$. The reformulated equivalent problem for each communication round reduces to:

$$\begin{aligned} \min_{l_{i,j}^{\mathrm{D2U}}[t], l_{j,\mathbf{c}}^{\mathrm{U2C}}[t]} \quad & \epsilon_{i,j}[t] + \epsilon_{j,\mathbf{c}}[t] \\ \text{s.t.} \quad & l_{i,j}^{\mathrm{D2U}}[t] + l_{j,\mathbf{c}}^{\mathrm{U2C}}[t] \leq M_{\mathrm{tot}}, \\ & l_{i,j}^{\mathrm{D2U}}[t] \geq L_1^b[t], \quad l_{j,\mathbf{c}}^{\mathrm{U2C}}[t] \geq L_2^b[t]. \end{aligned} \tag{34}$$

Critical analysis of the objective function's monotonicity reveals that its first derivative remains negative across the feasible domain, indicating an inverse relationship between blocklength allocation and error probability. Consequently, the Pareto-optimal solution resides at the constraint boundary defined by Eq. (34), enabling the substitution $l_{j,\mathbf{c}}^{\mathrm{U2C}}[t] = M_{\mathrm{tot}} - l_{i,j}^{\mathrm{D2U}}[t]$. This parametric reduction transforms the bivariate optimization into a univariate problem with $l_{i,j}^{\mathrm{D2U}}[t]$ as the sole decision variable, bounded above by $U_1^b[t] = M_{\mathrm{tot}} - L_2^b[t]$. The composite objective function thus becomes:

$$\begin{aligned} & f_{\mathrm{obj}}\left(l_{i,j}^{\mathrm{D2U}}[t], \Xi_{\mathrm{QoS}}\right) \\ & \quad = \mathbf{H}\left(f\left(l_{i,j}^{\mathrm{D2U}}[t]\right)\right) + \mathbf{H}\left(f\left(M_{\mathrm{tot}} - l_{i,j}^{\mathrm{D2U}}[t]\right)\right) \\ & \quad + \underbrace{\lambda_\Xi \cdot \Xi_{\mathrm{QoS}} \cdot \left(\max\left(0, \xi_{\mathrm{th}} - \xi_{\mathrm{achieved}}\right)\right)^2}_{\text{QoS penalty term}}, \end{aligned} \tag{35}$$

where $\mathbf{H}(\cdot)$ preserves the convexity properties established in prior analysis, $\Xi_{\mathrm{QoS}} \in [0,1]$ is a normalized QoS compliance factor that penalizes deviations from target QoS thresholds, ξ_{th} is the predefined QoS threshold, ξ_{achieved} is the empirically measured QoS performance, and λ_Ξ is a regularization parameter that balances entropy maximization and QoS adherence. To efficiently solve this constrained unimodal optimization, we implement the golden section algorithm-a robust derivative-free method particularly suited for integer-variable optimization in resource allocation scenarios. As detailed in Alg. 1, this approach iteratively narrows the search interval $\left[L_1^b[t], U_1^b[t]\right]$ through proportional partitioning, achieving superlinear convergence while maintaining computational tractability. The method's inherent stability and minimal function evaluation requirements make it ideally suited for real-time implementation in UAV-assisted networks, where $l_{i,j}^{\mathrm{D2U}}[t]$ and $l_{j,\mathbf{c}}^{\mathrm{U2C}}[t]$ represent discrete channel resource blocks subject to dynamic QoS constraints. Specifically, Alg. 1 outlines an iterative optimization algorithm designed to jointly optimize blocklength assignments and UAV trajectories to enhance communication efficiency while ensuring robustness. The algorithm begins by initializing parameters and iteratively refines blocklengths using a modified golden-section search method within nested loops. For each time step, it dynamically adjusts intervals based on computed error rates, balancing quality of service metrics and auxiliary parameters. Post-blocklength optimization, it updates UAV trajectories through a system of equations to ensure alignment with communication objectives. A secondary while-loop integrates robust gradient ascent for trajectory refinement, with adjustments driven by auxiliary matrices and exponential decay functions to evaluate trajectory quality. Final convergence checks ensure summative blocklength constraints and error thresholds are met, culminating in an optimized solution that balances spectral efficiency, error margins, and UAV positioning.

B. UAV Trajectory Optimization

To rigorously address the non-convex trajectory optimization challenge in the secondary subproblem, we focus on optimizing UAV positional vectors $\mathbf{q}_{\mathrm{uav}}[t]$ while maintaining fixed resource allocation parameters $\left\{l_{i,j}^{\mathrm{D2U}}[t], l_{j,\mathbf{c}}^{\mathrm{U2C}}[t], p_{i,j}^{\mathrm{D2U}}[t], p_{j,\mathbf{c}}^{\mathrm{U2C}}[t]\right\}$. The reformulated problem becomes:

$$\begin{aligned} & \min_{\mathbf{q}_{\mathrm{uav}}, b_j^{\mathrm{aux}}} \frac{1}{T}\sum_{t=1}^{T} \epsilon_{j,\mathbf{c}}[t] \\ & \text{s.t.} \quad (26\mathrm{a}), (26\mathrm{c}), (26\mathrm{d}), (26\mathrm{f}). \end{aligned} \tag{36}$$

The intrinsic non-convexity stems from both the composite Eq. (26) objective function and constraint, which involves coupled spatial-temporal relationships between UAV positions

Algorithm 1 Joint Blocklength and Trajectory Optimization

Input: $L_1^b, L_2^b, M_{\text{tot}}, \epsilon_{i,j}^{\max}, \epsilon_{j,\mathbf{c}}^{\max}, \mathbf{q}_{\text{uav}}^{j,I}, \mathbf{q}_{\text{uav}}^{j,F}, V_{max}$, blocklength limitation $\text{Lmt}_{\text{blok}}^1, \text{Lmt}_{\text{blok}}^2$, trajectory limitation $\text{Lmt}_{\text{traj}}, \forall j \in \mathbf{U}, \forall i \in \mathbf{D}$, auxiliary parameters $\Xi_{\text{QoS}}, \xi_{\text{th}}, \xi_{\text{achieved}}$, max iterations $\text{K}_{\max}$.

Output: $l_{j,\mathbf{c}}^{\text{U2C}}, l_{i,j}^{\text{D2U}}, \mathbf{q}_{\text{uav}}^j$.

Initialize: $\boldsymbol{l}^{(0)}, \mathbf{p}^{\mathbf{c}}, \mathbf{q}_{\text{uav}}^{j,0}, \mathbf{H}(\cdot)$, $\phi = \frac{1+\sqrt{5}}{2}$, $\ell = 1$, $k = 1$, $V_{\text{cu}}^0 = V_{\text{traj}}^0 = \infty$, $V_{\text{cu}}^1 = \frac{1}{T}\sum_{t=1}^{T} \epsilon_{j,c}[t]$, $V_{\text{traj}}^1 = \exp\left(-\frac{\Xi_{\text{QoS}}(\max(0,\xi_{\text{th}}-\xi_{\text{achieved}}))^2}{T}\sum_{t=1}^{T}\hat{\epsilon}_{j,\mathbf{c}}\right)$
while $\ell \le \text{K}_{\max}$ **and** ($|V_{\text{cu}}^{\ell} - V_{\text{cu}}^{\ell-1}| > \text{Lmt}_{\text{blok}}^1$ **or** $|V_{\text{traj}}^{\ell} - V_{\text{traj}}^{\ell-1}| > \text{Lmt}_{\text{traj}}$) **do**
  for $t = 1, \ldots, T$ **do**
    $a = L_1^b[t], \quad b = M_{\text{tot}} - L_2^b[t]$
    $c = b - \frac{(b-a)}{\phi}, \quad d = a + \frac{(b-a)}{\phi}$
    while $|c - d| > \text{Lmt}_{\text{blok}}^2$ **do**
      if $f_{\text{obj}}(c, \Xi_{\text{QoS}}) < f_{\text{obj}}(d, \Xi_{\text{QoS}})$ **then**
        Narrow interval towards minimum $b \leftarrow d$
      else
        $a \leftarrow c$
      end if
      Update c, d using ϕ
    end while
    $\text{tmp\_}^{(\ell)} \leftarrow \frac{b+a}{2}$
    $l_{i,j}^{\text{D2U}} \leftarrow \arg\min f_{\text{obj}}(\text{tmp\_}^{(\ell)})$
    Resource conservation $l_{j,\mathbf{c}}^{\text{U2C}} \leftarrow M_{\text{tot}} - l_{i,j}^{\text{D2U}}$
  end for
  $\mathbf{q}_{\text{uav}}^{j,\ell+1} \leftarrow$ solve Eq. (40)
  Convergence Check:
  $V_{\text{cu}}^{\ell+1} \leftarrow \frac{1}{T}\sum_{t=1}^{T} \epsilon_{j,\mathbf{c}}[t]$
  $V_{\text{traj}}^{\ell+1} \leftarrow \exp(-\frac{\Xi_{\text{QoS}}(\max(0,\xi_{\text{th}}-\xi_{\text{achieved}}))^2}{T}\sum_{t=1}^{T}\hat{\epsilon}_{j,\mathbf{c}})$
  $\ell \leftarrow \ell + 1$
end while
Final Constraints Verification:
if $\sum_j l_{j,\mathbf{c}}^{\text{U2C}} \le 1 - \sum_{i,j} \epsilon_{i,j}^{\max}$ **then**
  Return $l_{j,\mathbf{c}}^{\text{U2C}}, l_{i,j}^{\text{D2U}}, \mathbf{q}_{\text{uav}}^j$
else
  Throw "Infeasible: Constraints not met."
end if

and channel conditions. To mitigate this, we introduce convex-relaxed distance variables $d_{i,j}^{\text{D2U}}[t] \ge \|\mathbf{q}_{\text{uav}}^j[t] - \mathbf{q}_{\text{uav}}^i\|^2 + H^2$ and $d_{j,\mathbf{c}}^{\text{U2C}}[t] \ge \|\mathbf{q}_{\text{uav}}^j[t] - \boldsymbol{w}\|^2 + H^2$, where equality holds at optimality due to the error probability's monotonic relationship with propagation distance. Through rigorous convex analysis, we establish that the error components

$$E_{i,j}(d_{i,j}^{\text{D2U}}[t]) = \mathbf{H}(B_{i,j}[t](\log_2(1 + \frac{A_{i,j}[t]}{d_{i,j}^{\text{D2U}}[t]}) - C_{i,j}[t])), \quad (37)$$

$$E_j(d_{j,\mathbf{c}}^{\text{U2C}}[t]) = \mathbf{H}(B_{j,\mathbf{c}}[t](\log_2(1 + \frac{A_{j,\mathbf{c}}[t]}{d_{j,\mathbf{c}}^{\text{U2C}}[t]}) - C_{j,\mathbf{c}}[t])), \quad (38)$$

maintain concave profiles with respect to their distance variables, where $A_{i,j}[t] = p_{i,j}[t]\beta_0, B_{i,j}[t] = \ln(2)\sqrt{l_{i,j}^{\text{D2U}}[t]}$, and $C_{i,j}[t] = L/l_{i,j}^{\text{D2U}}[t]$. Employing SCA algorithm, we construct a surrogate objective function through first-order Taylor expansions at reference points $(\hat{d}_{i,j}^{\text{D2U}}[t], \hat{d}_{j,\mathbf{c}}^{U2C}[t])$:

$$\begin{aligned}\hat{\epsilon}_{j,\mathbf{c}}[t] = E_{i,j}(\hat{d}_{i,j}^{\text{D2U}}[t]) + \frac{\partial E_{i,j}}{\partial d_{i,j}^{\text{D2U}}}\Big|_{\hat{d}_{i,j}^{\text{D2U}}[t]} (d_{i,j}^{\text{D2U}}[t] - \hat{d}_{i,j}^{\text{D2U}}[t]) \\ + E_{j,\mathbf{c}}(\hat{d}_{j,\mathbf{c}}^{\text{U2C}}[t]) + \frac{\partial E_{j,\mathbf{c}}}{\partial d_{j,\mathbf{c}}^{\text{U2C}}}\Big|_{\hat{d}_{j,\mathbf{c}}^{\text{U2C}}[t]} (d_{j,\mathbf{c}}^{\text{U2C}}[t] - \hat{d}_{j,\mathbf{c}}^{\text{U2C}}[t]).\end{aligned} \quad (39)$$

This expansion provides a tight upper bound $\epsilon_{j,\mathbf{c}}[t] \le \hat{\epsilon}_{j,\mathbf{c}}[t]$, enabling convex reformulation of the original problem. For constraint Eq. (26a), we systematically address its dual manifestations through directional convex relaxations. The upper-bounding formulation is $\zeta_{\text{Er}} - \text{Er}_j + \text{G}_j^{\text{cu}}\left(\mathbf{q}_{\text{uav}}^j\right) \le \text{F}_j^{\text{cu}}\left(b_j^{\text{aux}}\right)$ using SCA at reference point $\hat{b}_j^{\text{aux}}$: $\text{F}_j^{\text{cu}}(b_j^{\text{aux}}) \ge \text{F}_j^{\text{cu}}(\hat{b}_j^{\text{aux}}) + \nabla\text{F}_j^{\text{cu}}(\hat{b}_j^{\text{aux}})^\top(b_j^{\text{aux}} - \hat{b}_j^{\text{aux}})$. In addition, we have lower-bounding formulation as $\text{F}_j^{\text{cu}}(b_j^{\text{aux}}) \le \text{G}_j^{\text{cu}}(\mathbf{q}_{\text{uav}}^j)$ with SCA at reference trajectory $\hat{\mathbf{q}}_{\text{uav}}^j$ as $\text{G}_j^{\text{cu}}(\mathbf{q}_{\text{uav}}^j) \ge \text{G}_j^{\text{cu}}(\hat{\mathbf{q}}_{\text{uav}}^j) + \nabla\text{G}_j^{\text{cu}}(\hat{\mathbf{q}}_{\text{uav}}^j)^\top(\mathbf{q}_{\text{uav}}^j - \hat{\mathbf{q}}_{\text{uav}}^j)$. The complete convexified problem becomes:

$$\begin{aligned}&\min_{\substack{\mathbf{q}_{\text{uav}}, b_j^{\text{aux}}, \\ d_{i,j}^{\text{D2U}}, d_{j,\mathbf{c}}^{\text{U2C}}}} \frac{1}{T}\sum_{t=1}^{T}\hat{\epsilon}_{j,\mathbf{c}}[t] \\ &\text{s.t. } \|\mathbf{q}_{\text{uav}}^j[t] - \mathbf{q}_{\text{uav}}^i\|^2 + H^2 \le d_{i,j}^{\text{D2U}}[t], \quad \forall t, i, j, \\ &\quad \|\mathbf{q}_{\text{uav}}^j[t] - \boldsymbol{w}\|^2 + H^2 \le d_{j,\mathbf{c}}^{\text{U2C}}[t], \quad \forall t, j, \\ &\quad d_{i,j}^{\text{D2U}}[t] \le \frac{A_{i,j}[t]}{2^{C_{i,j}[t] + \frac{\mathbf{H}^{-1}(\epsilon_{i,j}^{\max})}{B_{i,j}[t]}} - 1}, \\ &\quad d_{j,\mathbf{c}}^{\text{U2C}}[t] \le \frac{A_{j,\mathbf{c}}[t]}{2^{C_{j,\mathbf{c}}[t] + \frac{\mathbf{H}^{-1}(\epsilon_{j,\mathbf{c}}^{\max})}{B_{j,\mathbf{c}}[t]}} - 1}, \\ &\quad (26\text{b}), (26\text{c}), (26\text{d}), (26\text{f}).\end{aligned} \quad (40)$$

Transmission powers $p_{i,j}^{\text{D2U}}[t]$ and $p_{j,\mathbf{c}}^{\text{U2C}}[t]$ are maintained as fixed parameters derived from their theoretical lower bounds:

$$p_{i,j}^{\text{D2U}}[t] \ge \frac{2^{(\epsilon_{i,j}/A_{i,j}[t]) + B_{i,j}[t]} - 1}{h_{i,j}^{\text{D2U}}}, \quad (41)$$

$$p_{j,\mathbf{c}}^{\text{U2C}}[t] \ge \frac{2^{(\epsilon_{j,\mathbf{c}}/A_{j,\mathbf{c}}[t]) + B_{j,\mathbf{c}}[t]} - 1}{h_{j,\mathbf{c}}^{\text{U2C}}}, \quad (42)$$

where $A_{i,j}[t] = \log(2)\sqrt{l_{i,j}^{\text{D2U}}[t]}$, $B_{i,j}[t] = L/l_{i,j}^{\text{D2U}}[t]$, $A_{j,\mathbf{c}}[t] = \log(2)\sqrt{l_{j,\mathbf{c}}^{\text{U2C}}[t]}$, and $B_{j,\mathbf{c}}[t] = L/l_{j,\mathbf{c}}^{\text{U2C}}[t]$. This formulation guarantees feasibility while enabling efficient optimization through iterative convex programming techniques.

C. Local Update Weights Optimization

To rigorously address the non-convex optimization challenges in problem Eq. (26), we leverage our derived error probabilities $\epsilon_{j,\mathbf{c}}$ and $\epsilon_{i,j}$ corresponding to $\text{P}_{n,\mathbf{c}}^{\text{suc}}$ and $\text{P}_{m,n}^{\text{suc}}$ respectively. The core optimization task involves tuning the coordination matrix $\boldsymbol{\Psi}$ to minimize the upper-bounded variance metric while satisfying the critical resource normalization constraint in Eq. (26i). Recognizing the non-convexity induced by the bilinear term $\sum_{m,k\in\mathbf{S}_{\text{all}}} \text{P}_{m,k}^{\text{suc}}\text{P}_{k,m}^{\text{suc}}\left(E_{\{m,k\}} - \text{P}_{m,k}^{\text{suc}}\text{P}_{k,m}^{\text{suc}}\right)\psi_{m,k}\psi_{k,m}$,

where $\neg(m \in \mathbf{D} \wedge k \in \mathbf{D})$, we employ the arithmetic-geometric mean inequality $\psi_{m,k}\psi_{k,m} \leq \frac{1}{2}\left(\psi_{m,k}^2 + \psi_{k,m}^2\right)$ to construct a convex surrogate $\overline{\mathcal{Z}}(\mathbf{\Psi})$. Let $\mathbf{\Psi}_m = (\psi_{1,m}, \ldots, \psi_{c(\mathbf{S}_{\text{all}}),m})^T$ denote the m-th column of the coordination matrix. Exploiting the column-wise separability of (44), we implement a block-coordinate Gauss-Seidel algorithm with asynchronous updates. For the ℓ'-th iteration, the update rule for column m follows:

$$\mathbf{\Psi}_m^{(\ell'+1)} = \delta_m^{(\ell'+1)}\widehat{\mathbf{\Psi}}_m^{(\ell'+1)} + (1-\delta_m^{(\ell'+1)})\mathbf{\Psi}_m^{(\ell')}, \tag{43}$$

where the activation indicator $\delta_m^{(\ell'+1)}$ implements cyclic coordinate selection modulo $c(\mathbf{S}_{\text{all}})$. The column-wise optimization subproblem is:

$$\begin{aligned}
&\arg\min_{\widehat{\mathbf{\Psi}}_m} \sum_{n\in\mathbf{S_{all}}} \mathrm{P}_{n,\mathbf{c}}^{\text{suc}}\mathrm{P}_{m,n}^{\text{suc}}(1-\mathrm{P}_{n,\mathbf{c}}^{\text{suc}}\mathrm{P}_{m,n}^{\text{suc}})\psi_{n,m}^2 \\
&+2\sum_{k\in\mathbf{S_{all}}\setminus\{m,n\}}\sum_{n\in\mathbf{S_{all}}} \mathrm{P}_{n,\mathbf{c}}^{\text{suc}}(1-\mathrm{P}_{n,\mathbf{c}}^{\text{suc}})\mathrm{P}_{m,n}^{\text{suc}}\mathrm{P}_{k,n}^{\text{suc}}\psi_{n,m}\psi_{n,k}^{(\ell')} \\
&+\sum_{n\in\mathbf{S_{all}}} \mathrm{P}_{m,n}^{\text{suc}}\mathrm{P}_{n,\mathbf{c}}^{\text{suc}}\left(E_{\{m,n\}} - \mathrm{P}_{m,n}^{\text{suc}}\mathrm{P}_{n,m}^{\text{suc}}\right)\psi_{n,m}^2 \qquad (44)\\
&\text{s.t.} \sum_{n\in\mathbf{S_{all}}} \mathrm{P}_{n,\mathbf{c}}^{\text{suc}}\mathrm{P}_{m,n}^{\text{suc}}\psi_{n,m} = 1, \\
&\quad \left|\{\text{Var}\in\{m,n,k\} : \text{Var}\in\mathbf{D}\}\right| \leq 1.
\end{aligned}$$

The closed-form solution, $\widehat{\mathbf{\Psi}}_m^{(\ell'+1)}$, derived via Lagrangian duality with non-negativity constraints, can be expressed as Eq. 45 The dual variable λ_m is computed via bisection over Eq. 46. This structured approach guarantees monotonic improvement of the convex surrogate objective while maintaining feasibility through projection operations, ultimately converging to a stationary point of the original non-convex problem.

Algorithm 2 UAV-Cooperative Federated Learning

Input: $\mathbf{S}_{\text{all}}$, $\mathbf{q}_{\text{uav}}$, $\mathrm{P}_{m,n}^{\text{suc}}$, $\mathrm{P}_{m,\mathbf{c}}^{\text{suc}}$, Ξ_{QoS} , T, ζ_{Er} ;
Output: $\boldsymbol{v}^T$ and $\mathbf{\Psi}$;

```
Initialize: v^0 ← 0, p_1 ← P^suc_{m,c}, p_2 ← P^suc_{m,n}
for t = 0, 1, ..., T − 1 do
    Broadcast v^t to each device in S_all
    for each device m, n ∈ S_all and ¬(m ∈ D ∧ n ∈ D) do
        v_m^{t,0} ← v^t, ℓ ← 0
        while ℓ ≤ K do
            v_m^{t,ℓ+1} ← v_m^{(t,ℓ)} − ζ_t g_m(v_m^{(t,ℓ)})
            Ψ_m^{(ℓ+1)} = δ_m^{(ℓ+1)} Ψ̂_m^{(ℓ+1)} + (1 − δ_m^{(ℓ+1)}) Ψ_m^{(ℓ)}
            ℓ ← ℓ + 1
        end while
        Calculate Δv_m^{t+1} ← Eq. (13)
        Transmit v_m^{t+1} to each device in S_all
        if φ_{m,n}(t + 1) = 1 then
            Receive Δv_m^{t+1}
            Calculate ṽ_m^{t+1} ← Eq. (14)
        end if
        Upload Δṽ_m^{t+1} for aggregation
    end for
    if Receive Δv_m^{t+1} from device m ∈ S_all then
        φ_{m,c}(t + 1) ← 1
    else
        φ_{m,c}(t + 1) ← 0
    end if
    v_m^{t+1} ← Eq. (15)
end for
```

D. Discussion

The proposed scheme effectively mitigates non-IID issues through UAV cooperation by orchestrating dynamic data collection and transmission strategies. By optimizing UAV trajectories, the system actively reduces spatial data heterogeneity by prioritizing coverage of devices with underrepresented data patterns. For instance, UAVs adjust their flight paths to ensure balanced data acquisition from dispersed devices, which aligns local data distributions closer to the global dataset's statistical properties. This spatial coordination directly reduces the Kullback-Leibler divergence $\mathrm{KL}(\mathcal{D}_m \| \mathcal{D}_{\text{global}})$ between individual IoT devices' data and the aggregated global model. Moreover, the scheme employs adaptive resource allocation, where blocklength parameters are dynamically optimized based on device locations and channel conditions to minimize transmission errors. This ensures high-quality data uplink from remote devices, preventing their exclusion from the training process. Third, combined with client-weighting mechanisms, updates from devices with higher data reliability (lower error rates ϵ_i) and better IID properties are prioritized during model aggregation. Based on the convex optimization framework for transmission reliability and UAV trajectory control, we derive

$$\widehat{\mathbf{\Psi}}_m^{(\ell'+1)} = \begin{cases} \left(\dfrac{-2(1-\mathrm{P}_{n,\mathbf{c}}^{\text{suc}})\sum_{\substack{k\in\mathbf{S_{all}}\\k\neq m}} \mathrm{P}_{k,n}^{\text{suc}}\psi_{n,k}^{(\ell')} + \lambda_m}{2\left[(1-\mathrm{P}_{n,\mathbf{c}}^{\text{suc}}\mathrm{P}_{m,n}^{\text{suc}}) + \mathrm{P}_m^{\text{suc}}\left(E_{\{m,n\}}/\mathrm{P}_{m,n}^{\text{suc}} - \mathrm{P}_{n,m}^{\text{suc}}\right)\right]}\right)^+, & \text{if } \mathrm{P}_{n,\mathbf{c}}^{\text{suc}}\mathrm{P}_{m,n}^{\text{suc}} \in (0,1), \\ \dfrac{1}{\sum_{n\in\mathbf{S_{all}}} \mathbf{1}_{\{\mathrm{P}_{n,\mathbf{c}}^{\text{suc}}\mathrm{P}_{m,n}^{\text{suc}}=1\}}}, & \text{if } \mathrm{P}_{n,\mathbf{c}}^{\text{suc}}\mathrm{P}_{m,n}^{\text{suc}} = 1, \\ 0, & \text{otherwise.} \end{cases} \tag{45}$$

$$\left[0, \max_{\substack{n:\\ \mathrm{P}_{n,\mathbf{c}}^{\text{suc}}\mathrm{P}_{m,n}^{\text{suc}}\in(0,1)}} \left\{ \frac{2\left[(1-\mathrm{P}_{n,\mathbf{c}}^{\text{suc}}\mathrm{P}_{m,n}^{\text{suc}}) + \mathrm{P}_{m,n}^{\text{suc}}\left(E_{\{m,n\}}/\mathrm{P}_{m,n}^{\text{suc}} - \mathrm{P}_{n,m}^{\text{suc}}\right)\right]}{\mathrm{P}_{n,\mathbf{c}}^{\text{suc}}\mathrm{P}_{m,n}^{\text{suc}}} + 2(1-\mathrm{P}_{n,\mathbf{c}}^{\text{suc}}) \sum_{\substack{k\in\mathbf{S_{all}}\\k\neq m}} \mathrm{P}_{k,n}^{\text{suc}}\psi_{n,k}^{(\ell')} \right\}\right]. \tag{46}$$

This article has been accepted for publication in IEEE Transactions on Mobile Computing. This is the author's version which has not been fully edited and content may change prior to final publication. Citation information: DOI 10.1109/TMC.2026.3656974

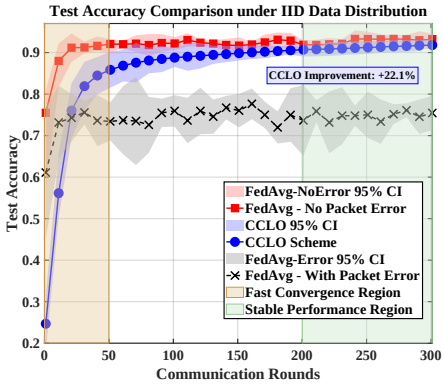

Fig. 3. Test accuracy over communication rounds under the IID data.

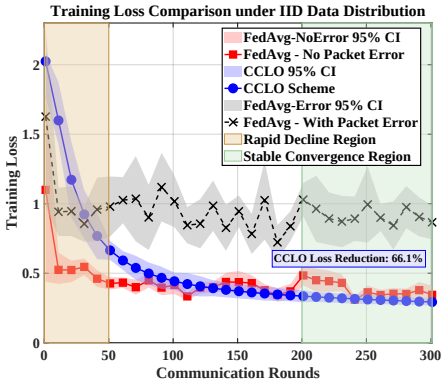

Fig. 4. Training loss over communication rounds under the IID data.

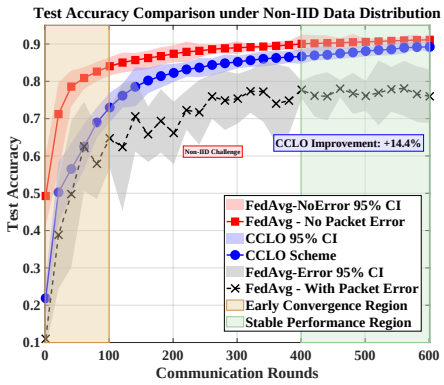

Fig. 5. Test accuracy over communication rounds under the Non-IID data.

the convergence inequality

$$\mathbb{E}\left[\mathcal{L}_m\left(\boldsymbol{v}_m;\mathcal{D}_m\right)\right]-\mathcal{L}_m\left(\boldsymbol{v}_m^*;\mathcal{D}_m\right) \leq \frac{C_1}{T}+\frac{C_2\sum_{m=1}^{c(\mathbf{S_{all}})}\mathcal{S}_m}{c(\mathbf{S_{all}})\sqrt{T}}-\beta_{\text{conv}}\cdot\text{Align}(\cdot), \quad (47)$$

where $\mathcal{S}_m$ is the local-global distribution discrepancy for device m,

$$\mathcal{S}_m=\mathbb{E}_{x\sim\mathcal{D}_m}\left[\text{KL}\left(\mathcal{D}_m\|\mathcal{D}_{\text{global}}\right)\right] +\left\|\nabla\mathcal{L}_m\left(\boldsymbol{v}_m;\mathcal{D}_m\right)-\nabla\mathcal{L}\left(\boldsymbol{v};\mathcal{D}_{\text{global}}\right)\right\|_2, \quad (48)$$

which is the sum of the divergence measuring statistical distribution mismatch and the gradient misalignment capturing optimization direction conflicts. Term C_1 is the baseline convergence constant which reflects deterministic factors independent of data heterogeneity, derived from initial model divergence and optimization step size, C_2 is the non-IID penalty coefficient which embodies the amplification effect of data heterogeneity on the convergence rate. The function $\text{Align}(\cdot)$ quantifies the feature alignment efficacy between local client models and the global model, implemented through gradient or feature space regularization. Specifically, for client i with model parameters $\boldsymbol{v}_m$, it enforces consistency by minimizing deviations in feature representations:

$$\text{Align}\left(\boldsymbol{v}_m\right)=\mathbb{E}_{x\sim\mathcal{D}_m}\left\|\text{Fr}_{\text{global}}-\text{Fr}_m\right\|^2, \quad (49)$$

where $\text{Fr}_{\text{global}}$ and Fr_m denote feature extractors of the global and local models, respectively. This regularization penalizes client-specific feature distribution shifts caused by non-IID data. Considering Eq. 47, only if β_{conv} scales inversely with data heterogeneity $\sum_{m=1}^{c(\mathbf{S_{all}})}\mathcal{S}_m$, it can be proved that the proposed scheme mitigates non-IID issues and accelerates global model convergence. When $\sum_{m=1}^{c(\mathbf{S_{all}})}\mathcal{S}_m$ increases, β_{conv} scales inversely ensuring clients with large $\mathcal{S}_m$ (high divergence from global data distribution) contribute less to aggregation. In addition, in the convergence bound $\frac{C_2\sum_{m=1}^{c(\mathbf{S_{all}})}\mathcal{S}_m}{c(\mathbf{S_{all}})\sqrt{T}}$, smaller β_{conv} counteracts high $\mathcal{S}_m$, lowering residual error terms and accelerating convergence toward the global optimum. To rigorously prove that the parameter β_{conv} scales inversely with data heterogeneity $\sum_{m=1}^{c(\mathbf{S_{all}})}\mathcal{S}_m$, we analyze the interplay between the convergence bound and the proposed mitigation mechanisms. The convergence inequality requires the mitigation gain term $\beta_{\text{conv}}\,\text{Align}(\cdot)$ to counteract the Non-IID penalty $\frac{C_2\sum_{m=1}^{c(\mathbf{S_{all}})}\mathcal{S}_m}{c(\mathbf{S_{all}})\sqrt{T}}$. Assuming the alignment effectiveness $\text{Align}(\cdot)\propto\frac{1}{\max_m\mathcal{S}_m}$ (a property of layer-wise feature map regularization in federated learning), substituting this relationship into the inequality yields $\beta_{\text{conv}}\propto\frac{(\max_m\mathcal{S}_m)^2}{\sqrt{T}}$. For large T, this simplifies to $\beta_{\text{conv}}=\mathcal{O}\left(1/\max_m\mathcal{S}_m\right)$, demonstrating the inverse proportionality. In addition, please refer to Appendix C for more details about the convergence sketch of the proposed tri-modular block-coordinate scheme.

V. PERFORMANCE EVALUATION

In this section, we present the simulation results to evaluate the performance of the proposed FL scheme. The FL system consists of $M=10$ devices and $N=5$ UAVs, randomly distributed within a $1000\ \text{m}\times1000\ \text{m}$ area, with a CS located at the center to facilitate communication. All UAVs operate at a fixed altitude of $H=100\ \text{m}$, while the laser transmitter used for powering the UAVs is positioned at $\mathbf{p^I}=[500,700]\text{m}$. The packet size is $L_{\text{pkt}}=130$ bits, with a total of 600 communication rounds, each lasting $\Delta_t=4$ seconds. The UAVs have a maximum velocity of $V_{\max}=25\ \text{m/s}$ and a mass of $\mu_n=15$ kg . To ensure continuous operation, the UAVs utilize a laser-powered energy harvesting system, with a laser beam spread of $\Delta\theta=3.4\times10^{-5}$ radians, an initial beam diameter of $S=0.1\ \text{m}$, a medium attenuation coefficient of $\alpha=10^{-6}\ \text{m}$, and a laser transmit power of $p^{\text{I}}=500\ \text{W}$. The energy storage capacity of UAV j is constrained between $\zeta_{\text{Er}}=10^3$ J and $\text{Er}_j=10^5$ J, with an RF chain efficiency of $\eta=1$. The packet error rate requirements are set to $\epsilon_{m,n}=10^{-5}$ for D2U communication and $\epsilon_n=10^{-6}$ for U2S transmissions to the CS.

The simulations are conducted using PyTorch-GPU 2.1.0 with Python 3.9 on a system featuring a 2.50 GHz Intel Core i5-10300H CPU, 16 GB of RAM, and an NVIDIA GTX 1650Ti GPU. A fully connected neural network is implemented for MNIST [28] classification, consisting of two dense layers followed by ReLU activations. The first layer includes 512 neurons, the second has 256 neurons, and the output layer, with 10 neurons, represents digit classes (0-9) using Softmax for class probability predictions. The model is trained using stochastic gradient descent (SGD) with a learning rate of 0.01, a batch size of 64, and cross-entropy loss to evaluate classification accuracy.

Figure 3 and 4 show the test accuracy and training loss, respectively, over communication rounds under an i.i.d. data distribution, while Fig. 5 and Fig. 6 show the corresponding results under a non-i.i.d. data distribution. In both scenarios, the proposed scheme demonstrates superior performance compared to FedAvg - with packet error, achieving significantly higher accuracy and lower training loss. Its performance closely approaches that of FedAvg - no packet error, which assumes ideal, error-free communication, highlighting the proposed scheme's ability to mitigate the effects of packet errors effectively. In contrast, FedAvg - with packet error shows the poorest performance, with consistently lower accuracy and higher, unstable training loss throughout the training process. These results validate the robustness of the proposed scheme in handling communication errors and maintaining reliable federated learning performance.

Figure 7 and 8 show the test accuracy and training loss for three strategies: Proposed, Fixed Blocklength Allocation, and Fixed UAV Trajectory under a non-i.i.d. data distribution. The proposed scheme achieves the highest test accuracy and lowest training loss, demonstrating the effectiveness of jointly optimizing blocklength allocation, power, and UAV trajectory. Fixed Blocklength Allocation outperforms Fixed UAV Trajectory but is limited by its inability to dynamically adjust blocklengths. The Fixed UAV Trajectory strategy performs the worst due to its failure to optimize UAV positions, resulting in higher error rates and less stable training. These results highlight the importance of optimizing both UAV trajectory and communication resources for robust FL performance.

Statistical significance is assessed across the IID and non-IID experiments by reporting 95% confidence intervals (CIs) as shaded bands in Fig. 3–Fig. 6 and Fig. 7–Fig. 8. In the stable convergence regime (after approximately 200 rounds), the CI bands of CCLO are separated from those of the error-prone or non-adaptive baselines: in Fig. 3 and Fig. 5, the lower bound of CCLO's 95% CI is positioned above the upper bound of FedAvg-with-error for most rounds, indicating that the observed accuracy improvements are unlikely to result from run-to-run randomness; similarly, in Fig. 4 and Fig. 6, CCLO's 95% CI is positioned below the corresponding baseline loss CIs after convergence, supporting that the loss reductions are statistically meaningful. Additionally, CCLO's CI bands become narrow in the stable region across these figures, suggesting low variance and stable convergence across independent runs, including under non-IID heterogeneity. For the ablation comparisons, Fig. 7 and Fig. 8 show that CCLO's performance advantages over fixed-trajectory and fixed-blocklength strategies are supported by non-overlapping 95% CIs in the stable region, confirming that the gains from joint reliability-and-coordination design are robust rather than incidental.

Figure 9 shows the test accuracy after 600 communication rounds for four FL strategies—Proposed, Fixed Blocklength Allocation, Fixed UAV Trajectory, and FedAvg—under varying PERs in a non-i.i.d. data setting. The proposed scheme consistently outperforms the others, achieving 92.27% accuracy at a PER of 0.05, compared to 90.54% for Fixed Blocklength Allocation, 87.72% for Fixed UAV Trajectory, and 91.04% for FedAvg. Even at a higher PER of 0.3, the proposed scheme maintains 89.35% accuracy, while Fixed Blocklength Allocation, Fixed UAV Trajectory, and FedAvg drop to 86.53%, 80.00%, and 77.45%, respectively. This highlights the effectiveness of joint optimization of blocklength, power allocation, and UAV trajectory in mitigating transmission errors, as opposed to the less adaptive Fixed Blocklength Allocation and the less robust Fixed UAV Trajectory and FedAvg strategies. These results emphasize the importance of joint optimization for robust FL performance in challenging IIoT conditions with non-i.i.d. data.

Figure 10 shows test accuracy at 600 communication rounds under varying blocklengths for three FL strategies: Proposed, Fixed Blocklength Allocation, and Fixed UAV Trajectory, in a non-i.i.d. data setting. As blocklengths increase from 250 to 450, all strategies improve, with the proposed scheme achieving 90.86% accuracy, outperforming Fixed Trajectory 86.79% and Fixed Blocklength Allocation 75.02%. These results highlight the importance of jointly optimizing blocklength, power allocation, and UAV trajectory for enhanced FL performance.

Figure 11 shows that increasing the number of UAVs accelerates convergence and lowers the final training loss. With five UAVs, the training loss decreases to around 0.021 after 600 communication rounds, compared to approximately 0.106 with one UAV. Training loss trends for three UAVs (0.074) and seven UAVs (0.1421) align with their respective test accuracy results, confirming that additional UAVs improve the stability and efficiency of training by mitigating unreliable communication. However, the diminishing returns beyond five UAVs suggest an optimal balance between performance improvements and costs.

Figures 12–15 demonstrate that the proposed CCLO framework consistently outperforms a broad set of representative baselines, including FedAvg, FedProx, SCAFFOLD, MOON, AHCS [29] and FedPKR [30], across both MNIST and CIFAR10 datasets. CCLO achieves 3–5$\%$ higher test accuracy and reduces the number of required communication rounds by approximately 8–12$\%$ compared with existing methods. The results indicate that the joint optimization of communication reliability and computation allocation in CCLO effectively minimizes the residual convergence term $\mathcal{Z}(\mathbf{p}_1, \mathbf{p}_2, \mathbf{\Psi})$, leading to faster early-stage convergence and more stable long-term accuracy.

Figure 16 and 17 show that CCLO maintains competitive performance under increasing non-IID severity (smaller β_{conv}) for both MNIST and CIFAR-10, outperforming FedAvg with packet errors and remaining on par with advanced baselines. To address the concerns regarding non-IID data distributions, data heterogeneity is quantified using the Dirichlet distribution parameter β, with smaller β values indicating higher levels of non-IID severity. MNIST dataset is utilized as a baseline benchmark, while CIFAR-10, characterized by greater intra-class variability, is employed to represent more complex scenarios. The evaluation results demonstrate that CCLO maintains robust performance as β decreases, consistently outperforming FedAvg in packet error conditions and achieving comparable accuracy relative to established baselines in-

This article has been accepted for publication in IEEE Transactions on Mobile Computing. This is the author's version which has not been fully edited and content may change prior to final publication. Citation information: DOI 10.1109/TMC.2026.3656974

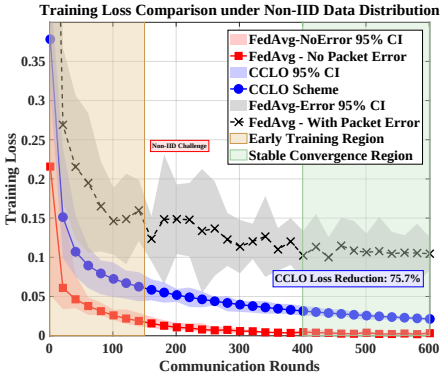

Fig. 6. Training loss over communication rounds under the Non-IID data.

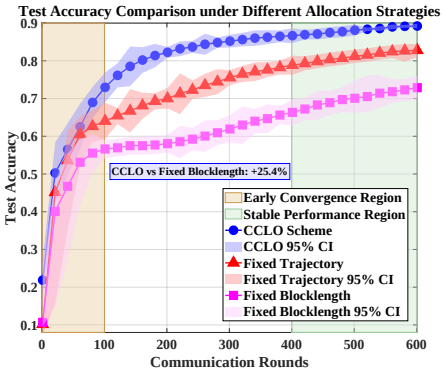

Fig. 7. Test accuracy over communication rounds for different FL schemes.

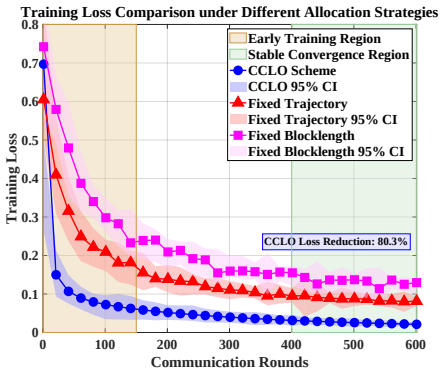

Fig. 8. Training loss over communication rounds for different FL schemes.

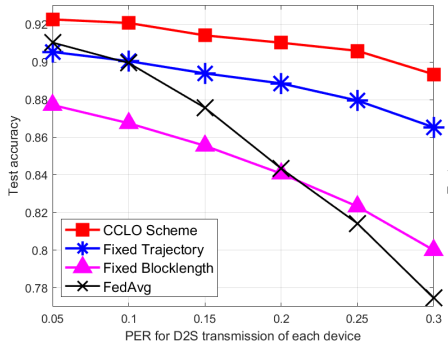

Fig. 9. Test accuracy at 600 communication rounds across various PERs.

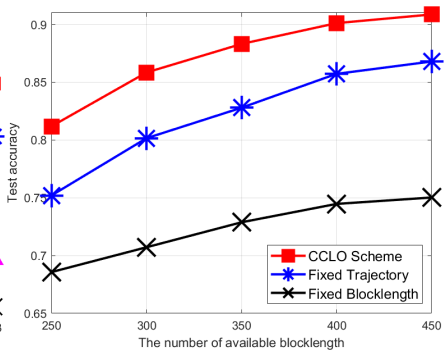

Fig. 10. Test accuracy at 600 communication rounds across various available blocklengths.

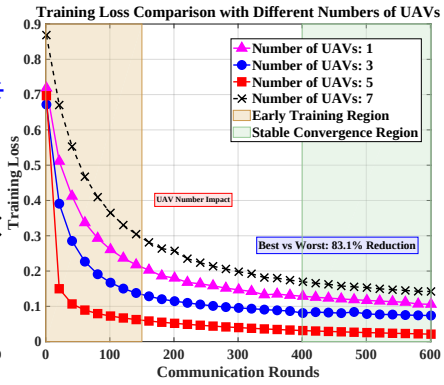

Fig. 11. Training loss over communication rounds under the Non-IID data distribution with different number of UAVs.

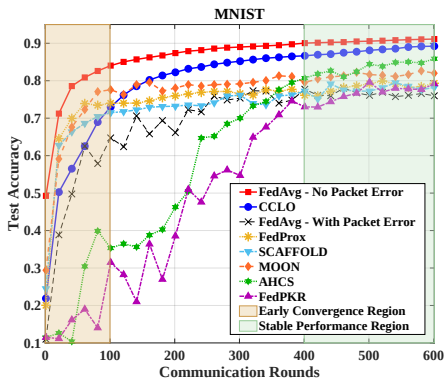

Fig. 12. Test accuracy comparison on MNIST among different schemes.

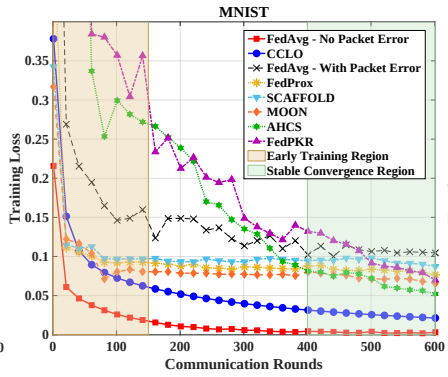

Fig. 13. Training loss comparison on MNIST among different schemes.

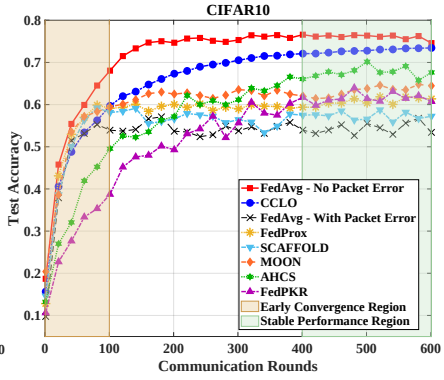

Fig. 14. Test accuracy comparison on CIFAR-10 among different schemes.

cluding AHCS and FedPKR. These findings validate CCLO's resilience across diverse heterogeneous data distributions.

VI. Conclusion

In this paper, we have presented a CCLO scheme aimed at addressing the intertwined challenges of delay, trajectory energy consumption, and model accuracy in UAV-assisted FL systems designed for Industrial IoT applications. Specifically, we designed a tri-modular approach encompassing dynamic blocklength allocation, energy-efficient trajectory planning, and reliability-aware weighting mechanisms. This integrated framework seeks to mitigate the impact of non-IID data on FL performance, while simultaneously ensuring robust communication reliability and effective resource utilization. Through extensive simulations, we demonstrated that the proposed CCLO framework not only reduces communication delay and decreases energy expenditure along UAV flight paths but also enhances the accuracy of the federated learning model by an average of 18.9% when benchmarked against conventional methodologies. We expect this work can further promote research interests in the delay-trajectory-accuracy trilemma optimization, whose significance will grow in UAV-cooperative FL-IoT systems as novel applications demand stringent balance among latency, energy,

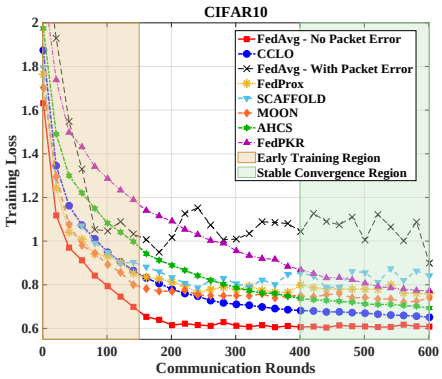

Fig. 15. Training loss comparison on CIFAR-10 among different schemes.

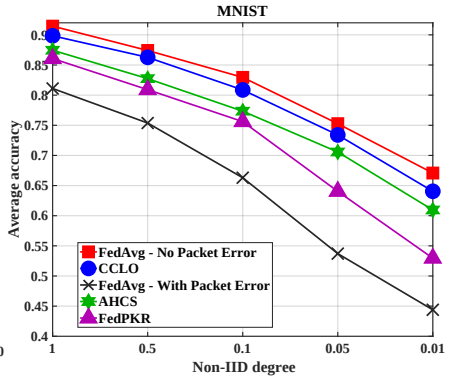

Fig. 16. Impact of data heterogeneity on average accuracy for MNIST.

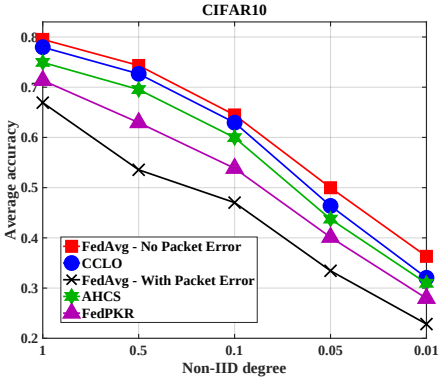

Fig. 17. Impact of data heterogeneity on average accuracy for CIFAR-10.

and model fidelity. Due to the escalating requirements of IoT deployments, next-generation UAV-assisted networks must evolve from static, single-objective designs to proactive, multi-dimensional frameworks that concurrently optimize delay bounds, trajectory efficiency, and learning accuracy. Achieving isolated performance targets is no longer sufficient; instead, harmonizing conflicting constraints has become imperative. For future work, we aim to investigate the tradeoff between network density, UAV mobility complexity, and the trilemma balance, particularly under ultra-dense IoT deployments with heterogeneous device distributions.

Acknowledgment

This work has been supported in part by the National Natural Science Foundation of China under Grant 62201148, in part by the Guangdong Province Basic and Applied Basic Research Foundation under Grant 2022KQNCX, in part by Dongguan Strategic Scientist Teams Project under Grant 20231900700022.

References

[1] P. Cao, L. Lei, S. Cai, G. Shen, X. Liu, X. Wang, L. Zhang, L. Zhou, and M. Guizani, "Computational Intelligence Algorithms for UAV Swarm Networking and Collaboration: A Comprehensive Survey and Future Directions," *IEEE Communications Surveys & Tutorials*, vol. 26, no. 4, pp. 2684–2728, 2024.

[2] J. Wang, J. Wang, Z. Tong, Z. Jiao, M. Zhang, and C. Jiang, "ACBFT: Adaptive Chained Byzantine Fault-Tolerant Consensus Protocol for UAV Ad Hoc Networks," *IEEE Transactions on Vehicular Technology*, vol. 74, no. 7, pp. 11 324–11 336, 2025.

[3] X. Hou, J. Wang, C. Jiang, Z. Meng, J. Chen, and Y. Ren, "Efficient Federated Learning for Metaverse via Dynamic User Selection, Gradient Quantization and Resource Allocation," *IEEE Journal on Selected Areas in Communications*, vol. 42, no. 4, pp. 850–866, 2024.

[4] Y. Xu, Y. Liao, L. Wang, H. Xu, Z. Jiang, and W. Zhang, "Overcoming Noisy Labels and Non-IID Data in Edge Federated Learning," *IEEE Transactions on Mobile Computing*, vol. 23, no. 12, pp. 11 406–11 421, 2024.

[5] X. Li, Y. Gao, Y. Deng, and X. Jiang, "Federated Learning With Adaptive Aggregation Weights for Non-IID Data in Edge Networks," *IEEE Transactions on Cognitive Communications and Networking*, pp. 1–1, 2025.

[6] J. Chen, C. Yi, S. D. Okegbile, J. Cai, and X. Shen, "Networking Architecture and Key Supporting Technologies for Human Digital Twin in Personalized Healthcare: A Comprehensive Survey," *IEEE Communications Surveys & Tutorials*, vol. 26, no. 1, pp. 706–746, 2024.

[7] Q. Wu, M. Cui, G. Zhang, F. Wang, Q. Wu, and X. Chu, "Latency Minimization for UAV-Enabled URLLC-Based Mobile Edge Computing Systems," *IEEE Transactions on Wireless Communications*, vol. 23, no. 4, pp. 3298–3311, 2024.

[8] Y. Tang, G. Zhu, W. Xu, M. H. Cheung, T.-M. Lok, and S. Cui, "Integrated Sensing, Computation, and Communication for UAV-assisted Federated Edge Learning," *IEEE Transactions on Wireless Communications*, pp. 1–1, 2025.

[9] M. Gkagkos, K. R. Narayanan, J.-F. Chamberland, and C. N. Georghiades, "FASURA: A Scheme for Quasi-Static Fading Unsourced Random Access Channels," *IEEE Transactions on Communications*, vol. 71, no. 11, pp. 6391–6401, 2023.

[10] Z. Ning, H. Ji, X. Wang, E. C. H. Ngai, L. Guo, and J. Liu, "Joint Optimization of Data Acquisition and Trajectory Planning for UAV-Assisted Wireless Powered Internet of Things," *IEEE Transactions on Mobile Computing*, vol. 24, no. 2, pp. 1016–1030, 2025.

[11] S. Zhang, Z. Ren, X. Li, Y. Long, J. Xu, and S. Cui, "Transmission Energy Allocation for Over-the-Air Computation with Energy Harvesting," *Journal of Communications and Information Networks*, vol. 9, no. 2, pp. 126–136, 2024.

[12] Q. Li, J. Chen, M. Cheffena, and X. Shen, "Channel-Aware Latency Tail Taming in Industrial IoT," *IEEE Transactions on Wireless Communications*, vol. 22, no. 9, pp. 6107–6123, 2023.

[13] M. L. Betalo, S. Leng, H. N. Abishu, A. M. Seid, M. Fakirah, A. Erbad, and M. Guizani, "Multi-Agent DRL-Based Energy Harvesting for Freshness of Data in UAV-Assisted Wireless Sensor Networks," *IEEE Transactions on Network and Service Management*, vol. 21, no. 6, pp. 6527–6541, 2024.

[14] X. Wang, M. Yi, J. Liu, Y. Zhang, M. Wang, and B. Bai, "Cooperative Data Collection With Multiple UAVs for Information Freshness in the Internet of Things," *IEEE Transactions on Communications*, vol. 71, no. 5, pp. 2740–2755, 2023.

[15] Y. Zhang, D. Liu, M. Duan, L. Li, X. Chen, A. Ren, Y. Tan, and C. Wang, "FedMDS: An Efficient Model Discrepancy-Aware Semi-Asynchronous Clustered Federated Learning Framework," *IEEE Transactions on Parallel and Distributed Systems*, vol. 34, no. 3, pp. 1007–1019, 2023.

[16] T. Li, A. K. Sahu, M. Zaheer, M. Sanjabi, A. Talwalkar, and V. Smith, "Federated Optimization in Heterogeneous Networks," in *Proc. of Machine Learning and Systems*, 2020, pp. 429–450.

[17] S. P. Karimireddy, S. Kale, M. Mohri, S. Reddi, S. Stich, and A. T. Suresh, "Scaffold: Stochastic Controlled Averaging for Federated Learning," in *Proc. of International Conference on Machine Learning*, vol. 119, 2020, pp. 5132–5143.

[18] J. Wang, Q. Liu, H. Liang, G. Joshi, and H. V. Poor, "Tackling the Objective Inconsistency Problem in Heterogeneous Federated Optimization," in *Proc. of NIPS*, 2020, pp. 7611–7623.

[19] W. Cheng, Y. Xiao, S. Zhang, and J. Wang, "Adaptive Finite Blocklength for Ultra-Low Latency in Wireless Communications," *IEEE Transactions on Wireless Communications*, vol. 21, no. 6, pp. 4450–4463, 2022.

[20] S. He, Z. An, J. Zhu, J. Zhang, Y. Huang, and Y. Zhang, "Beamforming Design for Multiuser uRLLC With Finite Blocklength Transmission," *IEEE Transactions on Wireless Communications*, vol. 20, no. 12, pp. 8096–8109, 2021.

[21] J. Zheng and K. Liu, "3D UAV Trajectory Planning With Obstacle Avoidance for UAV-Enabled Time-Constrained Data Collection Sys-

tems," *IEEE Transactions on Vehicular Technology*, vol. 74, no. 1, pp. 1460–1474, 2025.
[22] P. Qin, J. Li, J. Zhang, and Y. Fu, "Joint Task Allocation and Trajectory Optimization for Multi-UAV Collaborative Air–Ground Edge Computing," *IEEE Transactions on Network Science and Engineering*, vol. 11, no. 6, pp. 6231–6243, 2024.
[23] V. Balasubramanian, M. Aloqaily, and M. Reisslein, "Fed-TSN: Joint Failure Probability-Based Federated Learning for Fault-Tolerant Time-Sensitive Networks," *IEEE Transactions on Network and Service Management*, vol. 20, no. 2, pp. 1470–1486, 2023.
[24] T. Xiang, Y. Bi, X. Chen, Y. Liu, B. Wang, X. Shen, and X. Wang, "Federated Learning With Dynamic Epoch Adjustment and Collaborative Training in Mobile Edge Computing," *IEEE Transactions on Mobile Computing*, vol. 23, no. 5, pp. 4092–4106, 2024.
[25] P. Liu, Z. Li, J. Si, N. Al-Dhahir, and Y. Gao, "Joint Information-Theoretic Secrecy and Covertness for UAV-Assisted Wireless Transmission With Finite Blocklength," *IEEE Transactions on Vehicular Technology*, vol. 72, no. 8, pp. 10 187–10 199, 2023.
[26] Q. Li, Q. J. Ye, N. Zhang, W. Zhang, and F. Hu, "Digital-Twin-Enabled Industrial IoT: Vision, Framework, and Future Directions," *IEEE Wireless Communications*, pp. 1–9, 2025.
[27] Y. Polyanskiy, H. V. Poor, and S. Verdu, "Channel Coding Rate in the Finite Blocklength Regime," *IEEE Transactions on Information Theory*, vol. 56, no. 5, pp. 2307–2359, 2010.
[28] Y. LeCun, "The MNIST database of handwritten digits," Accessed: Sep. 2024. [Online]. Available: http://yann.lecun.com/exdb/mnist/.
[29] B. Luo, W. Xiao, S. Wang, J. Huang, and L. Tassiulas, "Adaptive Heterogeneous Client Sampling for Federated Learning Over Wireless Networks," *IEEE Transactions on Mobile Computing*, vol. 23, no. 10, pp. 9663–9677, 2024.
[30] J. Wang, R. Wang, G. Xu, D. He, X. Pei, F. Zhang, and J. Gan, "FedPKR: Federated Learning With Non-IID Data via Periodic Knowledge Review in Edge Computing," *IEEE Transactions on Sustainable Computing*, vol. 9, no. 6, pp. 902–912, 2024.

Qihao Li (M' 16) received his Ph.D. degree in University of Oslo, Norway, in 2019. After that, he was a postdoctoral fellow with the Department of Electrical and Computer Engineering, University of Waterloo, from 2019 to 2021, and a lecturer with the with the School of Electrical Engineering and Intelligentization, Dongguan University of Technology, from 2022 to 2023. Since 2023, he has been an assoicate professor at Jilin University, China. His current research focuses on industrial IoT, digital twin, intelligent agent networking and communication. He served as an Associate Editor for the IEEE Internet of Things Journal, a Guest Editor for the Future Internet Journal. He also servers/served as the workshop TPC Chair for IEEE VTC' 25, IEEE Globecom' 24, IEEE Infocom' 24, IEEE CIC/ICCC' 23-24, and members of TPC for several conferences. Dr. Li received the IEEE/CIC ICCC 2024 Best Paper Award, and the IEEE ICCT 2025 Young Scholar Award.

Tongzhou Yang (GS' 24) received the B.S. degree from the College of Communication Engineering, Jilin University, China, in 2024, where he is currently pursuing the Ph.D. degree. His current research interests include industrial IoT, federated learning, and digital twin.

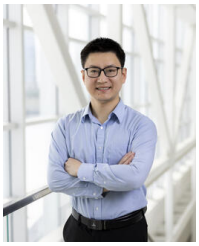

Qiang Ye (SM' 17) received the Ph.D. degree in electrical and computer engineering from the University of Waterloo, ON, Canada, in 2016. Since Sept 2023, he has been an Assistant Professor with the Department of Electrical and Software Engineering, Schulich School of Engineering, University of Calgary, AB, Canada. Before joining UCalgary, he worked as an Assistant Professor with the Memorial University of Newfoundland, NL, Canada (2021-2023) and with the Minnesota State University, Mankato, USA (2019-2021). He was with the Department of Electrical and Computer Engineering, University of Waterloo, as a Post-Doctoral Fellow and then a Research Associate (2016-2019). He has published around 80 research papers in top-ranked journals and conference proceedings. Dr. Ye serves as an Associate Editor for prestigious IEEE journals, such as IEEE IoT-J, TVT, TCCN, OJ-COMS. He received the Best Paper Award in the IEEE ICCC in 2024 and the IEEE TCCN Exemplary Editor Award in 2023. Dr. Ye received the Early Career Research Excellence Award, Schulich School of Engineering, University of Calgary, in 2024.

Cheng Nan received the B.E. and M.S. degrees from the Department of Electronics and Information Engineering, Tongji University, Shanghai, China, in 2009 and 2012, respectively, and the Ph.D. degree from the Department of Electrical and Computer Engineering, University of Waterloo, Waterloo, ON, Canada, in 2016. From 2017 to 2019, he was a Postdoctoral Fellow with the Department of Electrical and Computer Engineering, University of Toronto, Toronto, ON, Canada. He is currently a Professor with the State Key Laboratory of ISN and the School of Telecommunications Engineering, Xidian University, Xi'an, Shaanxi, China. He has authored or co-authored more than 90 journal papers in IEEE Transactions and other top journals. His research interests include B5G/6G, AI-driven future networks, and space-air–ground-integrated networks. Prof. Cheng is an Associate Editor of the IEEE Transactions on Vehicular Technology, IEEE Open Journal of the Communications Society, and Peer-to-Peer Networking and Applications. He is/was the guest editor of several journals.

Fengye Hu (M'12-SM'21) received the B.S. degree from the Department of Precision Instrument, Xi'an University of Technology (China) in 1996, and the M.S. and Ph.D. degrees in communication and information systems from Jilin University, China, in 2000 and 2007, respectively. He served as a visiting scholar in electrical and electronic engineering from Nanyang Technological University (NTU), Singapore, in 2011. He is currently a full professor in the College of Communication Engineering, Jilin University. His current research interests include wireless body area networks, wireless energy and information transfer, energy harvesting, cognitive radio, and space-time communication. He is an Editor of IEEE TVT, IEEE IOTJ, and China Communications, and served as an Editor of IET Communications.